PAPER No : 53

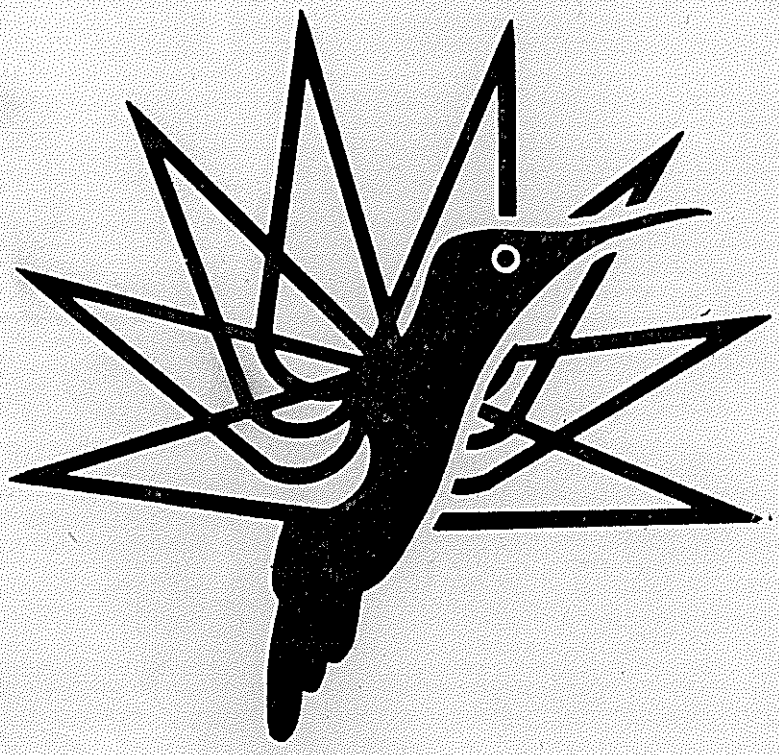

FEASIBILITY OF SIMPLIFYING COUPLED LAG-FLAP-TORSIONAL MODELS FOR ROTOR BLADE STABILITY IN FORWARD FLIGHT

BY

G. R. NEELAKANTAN

HINDUSTAN AERONAUTICS LIMITED
BANGALORE, INDIA

AND

G. H. GAONKAR

INDIAN INSTITUTE OF SCIENCE
BANGALORE, INDIA

TENTH EUROPEAN ROTORCRAFT FORUM

AUGUST 28 – 31, 1984 – THE HAGUE, THE NETHERLANDS

FEASIBILITY OF SIMPLIFYING COUPLED LAG-FLAP-TORSIONAL MODELS FOR ROTOR BLADE STABILITY IN FORWARD FLIGHT

G.R. Nilakantan,
Hindustan Aeronautics Limited,
Bangalore, India

G.H. Gaonkar
Indian Institute of Science,
Bangalore, India

SUMMARY

Feasibility of simplifying coupled lag-flap-torsional models is explored for the low-frequency stability of isolated hingeless rotor blades in forward flight. The non-linear equations of moderate deflections with appropriate geometric nonlinearities are valid to third order, so are the perturbed linear equations about time dependent equilibrium (trim) positions. Aerodynamic strip theory based on a quasi-steady approximation of two-dimensional unsteady airfoil theory is used. Under linear and quasilinear propulsive trim conditions, stability is investigated for four cases: a base-line model with elastic lag bending, flap bending and torsion degrees of freedom, the modified elastic lag-flap model that neglects only torsional dynamic effects, and the rigid blade models with and without quasisteady approximation to torsion. The method of equivalent Lock number and drag coefficient is used for qualitative insights into dynamic inflow effects. The range of validity of the modified elastic lag-flap and rigid lag-flap models is outlined with respect to torsional frequencies for soft (including matched stiffness) and stiff inplane rotors.

1. Introduction

Recently, much progress has been made in predicting low-frequency instabilities of hingeless rotorcraft in forward flight[1-3]. Such instabilities usually refer to single blade lag mode instability and to multi-blade lag regressing mode instabilities under hub-fixed and hub-free conditions. For most of these studies, the simplest model refers to the rigid lag-flap model with quasi-steady approximation to torsion and hub flexibility[1,4]. And, because of model simplicity, it was also relatively simpler to understand the importance of certain nonlinear terms, coupling parameters, trim positions and dynamic inflow.

However, for the stability analysis of isolated hingeless rotor blades with low torsional frequency (say, $\omega_\phi \leq 3$), an elastic coupled lag-flap-torsional or CLFT model is recommended; as discussed in reference 2 in hover and reference 3 in forward flight. Reference 2 also shows that except for blades with low torsional frequency, the bulk of the effects of torsion can be captured by including only the structural terms in the torsion equation (neglecting torsional dynamic effects). The feasibility of such a simplified model (modified elastic lag-flap model) under the analytically damanding conditions of forward flight has not been explored so far. Since a CLFT model analysis is available in forward flight[1,3] and since it is recommended for isolated blades with low torsional frequency[1-3], it is worthwhile to touch upon

the necessity and the feasibility of a simplified model.

A CLFT model intrinsically has a large number of degrees of freedom in multiblade lag mode stability analyses under hub-fixed and hub-free conditions and, to some extent, in single blade stability analysis as well. Such a model requires nonlinear equations that appropriately account for geometric nonlinearities associated with moderate deflections[1-3]. Further, perturbed linear equations require time dependent nonlinear equilibrium (trim) solutions[1,3,6]. Also, the Floquet analysis gives eigenmodes with frequency ambivalence and with diminished physical meaning. In general, the fewer the degrees of freedom, the simpler is the model synthesis, trimming and mode visibility[7,8]. It is expected that the complexity of the CLFT model practically precludes its use as a conceptual model, particularly for multiblade lag mode stability analyses. Past experience in multiblade analyses with the rigid lag-flap model with dynamic inflow or with the rigid flap-torsion model with active controls supports this expectation[4,9-12]. Further, in multiblade analyses, by comparison to single blade analysis, the lag regressing mode frequency is usually much less than the corresponding torsional regressing mode frequency[4,10]. Heuristically stated, with the use of a simplified model the error in single blade analysis should serve as an upper-bound on the error in multiblade analyses.

As for the feasibility of simplified models, it is explored comprehensively under forward flight conditions in the following respects:

1. The CLFT model is taken as the base-line or 'exact' model. The modified elastic lag-flap model without torsional dynamics is studied with respect to this base-line model for both soft and stiff inplane rotors in combination with low, intermediate and high torsional frequencies ($\omega_\phi < 3$, $3 \leq \omega_\phi \leq 5$, $\omega_\phi \geq 10$).

2. The stability of the base-line model also inlcudes the stiff inplane case with low torsional frequencies for $\mu > 0.25$ (when sudden degradation in stability is observed[3]), and the matched stiffness case (for which available lag mode damping data exhibit slight discrepancies in hover[2,15]).

3. For a reasonably comprehensive coverage of rotor blade models that vary from rigid to elastic blades, five models of increasing complexity are treated — two rigid lag-flap models without and with quasisteady approximation to torsion; the CLFT model with N = 1; the modified elastic lag-flap model with N = 2 and the base-line model (CLFT model with N = 2).

4. The effects of lag-flap structural coupling and equivalent kinematic pitch-lag and pitch-flap couplings are included. These couplings significantly influence stability, and for low pitch values, have almost identical physical significance with respect to rigid and elastic blades.

5. Dynamic inflow effects are included by the method of equivalent Lock number and drag coefficient. This method is used in the absence of a viable dynamic inflow model for rotors with one and two blades[13]. Inspite of the absence of regressing modes, it should provide qualitative insights into the effects of dynamic inflow.

6. The damping levels from the five models are presented for the propulsive trim condition with $\bar{f} = 0.01$ for (i) time-invariant linear steady state response of the rigid lag-flap models and (ii) time-variant quasi-linear steady state responses of the base-line model. Though such a presentation is an artifact due to using an equilibrium solution not intrinsic to a particular model, it provides an objective measure of direct comparison between the rigid and elastic blade models, without being biased by trim solutions.

II. Equations of Motion

The following is a brief account of generating the equations of motion, for details, e.g. ordering scheme etc. see reference 14. The manually derived nonlinear partial differential equations are checked term by term by symbolically generated equations using the method of reference 18.

The geometry of the rotor blade with the co-ordinate system and elastic displacements is shown in Figure 1. The main assumptions are: (a) the blade has uniform mass and stiffness distributions; (b) the blade has no pretwist; (c) chordwise offsets of the elastic axis, mass centre axis and aerodynamic centre axis are zero; (d) the aerodynamic forces are derived from a strip theory with a quasisteady approximation of two dimensional unsteady airfoil theory; (e) the blade undergoes moderate deflections and (f) the compressibility and stall effects are negligible. An essential feature of the derivation is that terms of the order $0(\varepsilon^3)$ are retained throughout, where ε is a small parameter of the order of bending slopes. The complete set of coupled lag-flap torsional equations of motion are given in reference 14. However, to stress the generality and complexity of the equations of motion, as an example, the lead-lag equation is given in Appendix A. The underlined terms in equation (A-1) correspond to the terms in the equations (B-4) and (B-6) given in reference 3 when chordwise offsets, precone, structural damping and hinge offsets are ignored. However, equations with precone are given in reference 14.

Solution of the Equations

The system of coupled nonlinear, partial differential equations of motion with periodic coefficients is transformed into a system of ordinary nonlinear differential equations by Galerkin's method. The elastic degrees of freedom, v, w and ϕ are expressed in terms of a series of generalized coordinates and mode shape functions as follows:

$$v = \sum_{j=1}^{N} V_j(\psi)\, \psi_j(x)$$

$$w = \sum_{j=1}^{N} W_j(\psi)\, \psi_j(x)$$

$$\phi = \sum_{j=1}^{N} \Phi_j(\psi)\, \psi_j(x)$$

The standard nonrotating, uncoupled mode shapes for a uniform beam are

assumed for the bending and torsional deflections[2]. In the analysis, two modes each for flap bending, lag bending and torsion are assumed. This results in six modal equations in terms of generalized co-ordinates v_1, v_2, w_1, w_2, ϕ_1 and ϕ_2.

Trim Procedure[3,6]

It is known that the solution of the aeroelastic stability equations in forward flight are inherently coupled with the trim state of the complete helicopter. In the present method, the trim state is obtained by performing a trim analysis under the following conditions: (a) only the first elastic flap mode is important; (b) all harmonics associated with the first flap mode are included as in reference 3; and (c) the helicopter is in straight and steady level flight condition. The control trim inputs refer to propulsive trim which simulates actual forward flight conditions[3]. The non-dimensional weight coefficient is assumed to be equal to the thrust coefficient. The vertical and horizontal force equilibrium and zero pitching and rolling moment conditions are maintained. Figure 2 shows typical control inputs under propulsive trim conditions.

Time Dependent Equilibrium Position, and Stability

To obtain the time dependent equilibrium position, the system of equations for the hingeless blade in forward is written in state variable form. The analysis is carried out for the linear system and the complete nonlinear system as given in reference 3. Once the time dependent equilibrium position is obtained, the stability of the system is studied by perturbing it about the corresponding equilibrium position. The squares of perturbation quantities are neglected. The stability of the linearized system is determined from Floquet theory using single pass approach[7].

The various parameter values used in the analysis are given in Table I, which also indicates the base-line configuration. Figures 3 and 4 show typical steady state response solutions for the blade tip. Figure 3 shows the response of the first flap mode for a soft inplane rotor for $\mu = 0.2$ with $\omega_v = 0.7$, $\omega_\phi = 5.0$ and $R = 1.0$. Three curves are depicted in Figures 3 and 4. The curve denoted as "rigid blade" shows the time invariant value obtained from the rigid blade analysis[8,9]. The curve denoted as "linear' corresponds to the linear periodic response obtained by neglecting all nonlinear terms. The curve, denoted as "quasi-linear" refers to the linearized response which corresponds to $K = 1$ according to reference 3, where K is an iteration index used in quasilinearization. The results obtained from the linearized response ($K = 1$) differed little from those obtained from the first approximation of the fully nonlinear response ($K = 2$). Therefore, only the linearized response ($K = 1$) values have been used in predicting stability. Figure 4 shows similar results for the first lag mode. It is seen that the nonlinear terms have a pronounced effect on the response, as observed in reference 3.

III. Bending-Torsion Structural Coupling

The treatment of equivalent kinematic pitch-flap and pitch-lag

Table I : BASE-LINE CONFIGURATION AND ADDITIONAL PARAMETER VALUES FOR NUMERICAL RESULTS

Parameters	Base-line Parameter Values	Additional Parameter Values
ω_v	0.7, 1.5	Variable
ω_w	1.15	--
ω_ϕ	2.5, 5.0, 10.0	Variable
μ	0.3	0.0 - 0.4
R	1.0	0.0, 0.5
k_m/R	0.025	--
k_{m_1}/k_{m_2}	0.0	--
$(k_A/k_m)^2$	1.5	--
γ	5.5	--
σ	0.07	--
C_W	0.005	--
c/R	$\pi/40$	--
c_{d_0}	0.01	--
Trim	$\bar{f} = 0.01$	--
N	2	1

couplings generated by the nonlinear structural bending torsion couplings is given in reference 2 for hover. An extension of this analysis under demanding conditions of forward flight is given in refernce 14. A brief account of this analysis follows; (for additional details see reference 14).

Consider the following structural terms in the torsion equation, viz.,

$$- GJ \left(\phi'' + w' v''' + v'' w''\right)$$

$$+ (EI_{z'} - EI_{y'}) \cos(2R\theta) \left(v'' w'' + \phi w'' w'' - \phi v'' v''\right)$$

$$+ (EI_{z'} - EI_{y'}) \sin(2R\theta) \left(\tfrac{1}{2} w'' w'' - \tfrac{1}{2} v'' v'' - 2\phi v'' w''\right) \quad \ldots\ldots (1)$$

The singly underlined terms correspond to those given in equation (38) of reference 2. Since v, w and ϕ are of the order $0(\varepsilon)$, the doubly underlined terms are at least $0(\varepsilon^2)$. Retaining all the terms in equations (1), the corresponding expressions for θ_β and θ_ζ are[14]:

$$\theta_\beta = \left[\frac{GJ}{m\,\Omega^2\,k_m^2\,\bar{R}^2} \{F_{111}\,V_{01} + G_{111}\,V_{01}\} \right.$$

$$- \frac{(EI_{z'} - EI_{y'})}{m\,\Omega^2\,k_m^2\,\bar{R}^2} \cos(2R\theta)\,(\underline{G_{111}\,V_{01}} + 2\,M_{1111}\,\phi_{01}\,W_{01})$$

$$\left. - \frac{(EI_{z'} - EI_{y'})}{m\,\Omega^2\,k_m^2\,\bar{R}^2} \sin(2R\theta)\,(\underline{G_{111}\,W_{01}} - 2\,M_{1111}\,\phi_{01}\,V_{01}) \right] \times \frac{1}{X}$$

$$\theta_\zeta = \left[\frac{GJ}{m\,\Omega^2\,k_m^2\,\bar{R}^2} (F_{111}\,W_{01} + G_{111}\,W_{01}) \right.$$

$$- \frac{(k_{m_2}^2 - k_{m_1}^2)}{k_{m_2}^2} 2\cos(2\theta)\,H_{111}\,\phi_{01}$$

$$- \frac{(EI_{z'} - EI_{y'})}{m\,\Omega^2\,k_m^2\,\bar{R}^2} \cos(2R\theta)\,(\underline{G_{111}\,W_{01}} - 2\,M_{1111}\,\phi_{01}\,V_{01})$$

$$\left. - \frac{(EI_{z'} - EI_{y'})}{m\,\Omega^2\,k_m^2\,\bar{R}^2} \sin(2R\theta)\,(\underline{-\,G_{111}\,V_{01}} - 2\,M_{1111}\,\phi_{01}\,V_{01}) \right] \times \frac{1}{X}$$

..... (2)

where $X = \omega_\phi^2 - 1 + \cos(2\theta)$

$$\omega_\phi^2 = \frac{k_{m_2}^2 - k_{m_1}^2}{k_m^2} + \frac{k_A^2}{k_m^2} N_{11} + \frac{GJ\,\pi^2}{4\,m\,\Omega^2\,k_m^2\,\bar{R}^2}$$

$$+ \frac{2\,(k_{m_2}^2 - k_{m_1}^2)}{k_m^2} H_{111}\,V_{01}\cos(2\theta),$$

$$F_{111} = \int \theta_1\,\psi_1'\,\psi_1'''\,dx, \qquad G_{111} = \int \theta_1\,\psi_1''\,\psi_1''\,dx,$$

$$H_{111} = \int \theta_1\,\psi_1'\,\theta_1\,dx, \qquad C_{11} = \int x\,\theta_1\,\psi_1\,dx,$$

$$M_{1111} = \int \theta_1^2\,\psi_1'^2\,dx \qquad D_{11} = \int \theta_1\,\psi_1'\,dx$$

The underlined terms in equation (2) correspond to those in equation (40) of reference 2.

In this analysis, θ_β and θ_ζ are computed at different azimuthal stations and then time averaged to yield equivalent θ_β and θ_ζ values for a particular advance ratio, μ. Figures 5a and 5b show the azimuthal variations of θ_β and θ_ζ for a soft inplane rotor with R = 1.0 and for μ = 0.1 and 0.4. The time averaged values of θ_β and θ_ζ are shown by do ted lines in Figures 5a and 5b. The value of θ_ζ remains negative at all azimuthal positions. However, the values of θ_β become positive over a small region around $\psi = 180^0$ for μ = 0.1. This region expands with increasing μ, see Figure 5b, for μ = 0.4. The Figures 6a and 6b present the time averaged values of θ_β and θ_ζ for soft and stiff inplane rotors for μ = 0.0 to 0.4 with R = 1.0. Figures 6a and 6b (R = 1) show that the time averaged values of θ_β and θ_ζ are smaller for soft inplane rotors compared to corresponding values of stiff inplane rotors. As expected, for high torsional frequencies, $\omega_\phi > 10$, the couplings become very small, whereas for very low torsional frequencies, $\omega_\phi < 3.0$, the couplings become large and dominant.

IV. Numerical Results

Numerical results primarily refer to the damping levels of the first lag mode which is a low frequency mode. For hingeless rotor blades, the low-frequency instability usually involves this mode near the fundamental lag bending natural frequency ω_v. Figure 7 shows the base-line configuration for both soft (ω_v = 0.7) and stiff (ω_v = 1.5) inplane rotors. For rotor blades, the fundamental torsional frequency or ω_ϕ usually varies from 3 to 8. Therefore, for illustration, we select ω_ϕ = 2.5 and 5 for the soft inplane case and ω_ϕ = 5 for the stiff inplane case. It should be pointed out that the numerical work presented in this paper forms only a fraction of the results in reference 14. The parameter R in Figure 7 represents flag-lag structural coupling, which varies from zero to one. For small pitch angles, R has the same connotation for both the CLFT models and for the rigid blade models (rigid flap-lag models without and with quasisteady approximation to torsion and hub flexibility). Therefore the same symbol R has been used to typify flap-lag coupling for both elastic and rigid blade models. The physical significance of R is extensively discussed in the literature; for example, see reference 2 for the elastic case and reference 5 for the rigid case. However, it is good to mention that a thorough treatment of flap-lag coupling to include hub flexibility is an involved problem and that the term 'hub' refers to the inboard position of the blade system which does not rotate with pitch. The inclusion of hub flexibility through the introduction of a single parameter R (replacing θ by Rθ only in the structural term of the blade equations) is a highly simplified means of including hub flexibility, no matter how sophisticated the blade representation is. Therefore, in the sequel, quantitative comparisons with the base-line configurations are used for convenience of discussion and they should be viewed only in the context of establishing valid trends concerning simplified CLFT models.

In Figure 7, since R varies from 0 to 1, we have used three values of R — 0.0, 0.5 and 1.0 — in combination with each value of ω_ϕ. It is seen that the first lag mode damping for a given ω_ϕ, shows almost identical trends for all the three values of R for both soft and stiff

inplane configurations. Therefore, for the remaining set of results we have taken R = 1, and additional data for R ≤ 1 are available in reference 14.

Another question that concerns the base-line configuration is the number of elastic modes. There is a substantial quantitative difference in the damping data, between the CLFT models with N = 1 and 2, although qualitatively both the models depict similar trends. Preliminary data show[14] that N > 2, this quantitative difference is not at all appreciable to warrant the use of a base-line configuration with more than two elastic modes for each degree of freedom. Therefore, in the present exploratory study we have taken N = 2 for the base-line configuration.

Thus far, we studied the first lag mode damping values of the base-line model for two discrete values of the fundamental lag frequency, ω_v. Since ω_v is an important parameter, it is equally instructive to continue this study over a continuous spectrum of ω_v values. Such a study is a valuable guide for exploring the feasibility of simplifying the base-line model, and it is taken up in Figures 8 to 10. For hover, Figure 8a with $\theta = 0.17$ shows identical trends when compared to Figure 44 of reference 2 for which $\theta = 0.3$. Thus, from the hovering case to $\mu = 0.1$ (Figure 8b) the lag damping increases with decreasing ω_ϕ, except for ω_ϕ values less than the matched stiffness values. For $\mu = 0.2$, as seen from Figure 9a, the variation in lag damping begins to show changing trends for the stiff inplane configuration. As a matter of fact for $\mu = 0.3$ (Figure 9b), the variation in lag damping is difficult to characterize in a simple way for the stiff inplane configuration. And from Figures 9b and 10 for which $\mu = 0.3$ and 0.4 respectively, we see that the case with $\omega_\phi = 2.5$ exhibits increasing destabilizing trend with increasing ω_v. It also appears that rotor blades with excessive torsional flexibility (say, $\omega_\phi \leq 3.0$) are not desirable for stiff inplane rotors for high speed flight regimes ($\mu \geq 0.25$). Figure 10 with $\mu = 0.4$ is basically an extrapolated version of Figure 9b with $\mu = 0.3$. The question natuaally arises as to why the torsionally flexible blade with $\omega_\phi = 2.5$ shows strongly destabilising trends with increasing μ in sharp contrast to the other two configurations with $\omega_\phi = 5$ and 10. A study of this question is taken up in Figure 11 which shows the first lag mode damping as a function of μ for various values of ω_ϕ. Figure 11 clearly shows that for $\omega_\phi = 2.5$, the damping level basically remains constant for $\mu \leq 0.2$ and it drops rather suddently, exhibiting abrupt degradation in stability margins in contrast to the cases with $\omega_\phi \geq 3.5$ for which lag mode damping slightly increases with increasing μ. For the intermediate case with $\omega_\phi = 3.0$, the damping level shows slighlly decreasing trend for $\mu > 0.3$. We also mention that the variation of lag damping of Figure 11 is consistent with an earlier study[3]; also see reference 14. Thus the data in Figure 11 basically confirm the unexpected variation in damping levels of blades which have excessive torsional flexibility, as depicted in Figure 10. Although the data in Figure 11 are consistent with those of Figures 9 and 10, it would require further investigation to explain physically why the damping level suddenly drops for $\mu > 0.2$ or so, for blades that are highly torsionally flexible for the stiff inplane configuration. According to reference 3, such a sudden degradation in stability is associated with the change in the sign of structural coupling terms when the model changes from the soft inplane configuration to the stiff inplane one. This explanation seems to merit further scrutiny since this sudden degradation in stability margins is associated with high advance ratio flight regimes. From Figures 6a and 6b, the

negative pitch-flap coupling shows a suddenly increasing trend only for the stiff inplane configuration for $\mu > 0.2$. It is generally recognised that negative pitch-flap coupling is destabilizing in forward flight. Thus, for the stiff inplane case, the increasing values of negative pitch-flap coupling for $\mu > 0.2$ might partly explain the sudden degradation in stability margins observed in Figure 11 for $\omega_\phi = 2.5$ and for $\mu > 0.2$.

Before we close the discussion of Figures 8 to 10, it is good to touch upon the matched stiffness case in some detail particularly in view of the findings of reference 15. For the matched stiffness case as seen from Figures 8 to 10, the lag mode damping levels are independent of torsional frequency both in hover and forward flight, as was the case in reference 2 in hover. In the present study, terms $0(\varepsilon^3)$ are retained throughout, whereas in reference 2, terms $0(\varepsilon^3)$ are retained only when they contribute to damping. Therefore, as seen from equation (2), θ_β and θ_ζ are not identically equal to zero in matched stiffness case, although non-zero values of θ_β and θ_ζ are of order $0(\varepsilon^3)$ which are of little computational consequence. In other words, the present study shows the same variation in lag damping for the matched stiffness case as in reference 2. However, in a recent study in hover[15], the damping level ocurves do not cross at the matched stiffness frequency values. This aspect of the problem is further being pursued.

After having studied the base-line configuration, we come to assessing the adequacy of two types of simplified models as possible alternatives to the base-line configuration. The first type refers to the simplified CLFT model or the modified flap-lag (MFL) model with quasi-steady approximation to torsion. The second type refers to the rigid blade model with and without quasisteady approximation to torsion. The data from Figure 12 to 21 refer to the adequacy of these simplified models in predicting first lag mode damping. The quasisteady approximation implies that torsional dynamic effects are neglected. For example, based on order of magnitude considerations, $\ddot{\phi}_j$ and $\dot{\phi}_j$ terms are neglected, but the dominant torsional structural stiffness terms are retained[14]. Such an approach provides a rational means of capturing most of the torsional effects without including torsion as an independent degree of freedom. From this approach lag-flap-torsion equations reduce to modified lag-flap equations, originally suggested for hovering in reference 2. For additional discussion see reference 14 which treats the forward flight case for a wide variety of hingeless rotor configurations, including details of algebraic manipulations as well.

Such simplified models offer promise for multiblade lag mode stability analyses under hub-fixed[11,12] and hub-free (aeromechanical stability) conditions[8,9]. For typical helicopters, the rotors are soft inplane[16] with $\omega_v \simeq 0.7$ and $\omega_\phi \simeq 5.0$, that is, the frequency margin (ω_ϕ/ω_v) is close to 7. In the multiblade analyses this margin increases to about 4/0.3 or 13. Thus, heuristically stated, the error in using the simplified models in the single blade analysis should serve as an upper board on the expected error in multiblade lag mode stability analyses. With such simplified models of a single blade, the inclusion of dynamic inflow, airframe coupling, control flexibility etc. in multiblade analyses become tractable in forward flight. For certain rotor configurations and operating conditions, such a simplified model may provide only qualitative approximations. However, the tractability of the simplified models may out-weigh this fact.

For assessing the adequacy of the MFL model, we come to Figures 12 to 14 and Figures 15 to 17 which pertain to soft and stiff inplane configurations respectively. Here, the damping data from the base-line model are compared with those from the MFL model. Figures 12 to 14 show that the MFL model provides an excellent approximation to the base-line model even for $\omega_\phi = 2.5$ (Figure 12). As expected, the accuracy of the MFL model increases with increasing ω_ϕ, see Figures 13 and 14. Thus, the MFL model provides a viable alternative to the base-line model for soft inplane rotors. Figure 15 shows similar comparison for the stiff inplane rotor for $\omega_\phi = 2.5$. It is seen that the MFL model fails to establish even qualitatively valid trends. However, for $\omega_\phi = 5.0$, as shown in Figure 16, the simpler model though quantitatively crude, does provide valid qualitative trends and the accuracy of this simple model increases with increasing ω_ϕ. For example, in Figure 17, for $\omega_\phi = 10.0$, the MFL model provides an excellent approximation to the base-line model. Thus, for the stiff inplane rotor, the MFL model is not satisfactory for $\omega_\phi \leq 3.0$ and it is satisfactory for $\omega_\phi \geq 5.0$.

In most of the analyses of aeromechanical stability[8,9,17] and of multiblade lag mode stability under hub-fixed conditions[11-13] the blade model is either a CLFT model with N = 1,[17] or a rigid blade model[8,9,11-13]. Therefore, it is of interest how far these two sets of models compare with the base-line configuration in predicting lag mode instability of a single blade. Such a comparison is taken up in Figures 18 to 21. For rigid blade models, the trim solutions are time invariant, whereas, for CLFT models, they are time variant. In the comparison process, we have used both the trim solutions for elastic and rigid blade models. The use of time invariant trim for elastic blade models and time variant trim for rigid blade models is at best an artifact. Nevertheless, such a two-fold comparison provides an objective measure of comparison with the base-line model and rules out the possibility that such a comparison process is biased by trim solutions.

In Figures 18 to 21, we have considered four cases — (i) base-line model, (ii) CLFT model with N = 1, (iii) rigid blade model with quasisteady approximation to torsion, and (iv) rigid blade model without torsion. While Figures 19, 20 and 21 use time variant trim solutions, Figure 18 uses time invariant trim solutions. Further, soft inplane condition ($\omega_v = 0.7$) is used in Figures 18 and 19, and stiff inplane condition ($\omega_v = 1.5$) is used in Figures 20 and 21.

Coming to Figure 18, we observe three points. First, the rigid blade model with quasisteady approximation to torsion is always better than the rigid blade model without torsion, and compares well with the CLFT model with N = 1. Second, those three models which are basically 'one-elastic-mode' models provide qualitatively valid trends but are quantitatively crude approximations to the base-line model. Third, somewhat unexpected, is the case with a high torsional frequency, $\omega_\phi = 10.0$. Even for this case, the simplified models are not appreciably different from the previous case with $\omega_\phi = 2.5$. This points to the fact that second flap bending, lag bending and torsion modes introduce appreciable effects which cannot be captured in the simplified models. It should also be mentioned that nonlinear effects in the CLFT momel with N = 2 are relatively more premodinant when compared to the CLFT model with N = 1.

Figure 19 with $\omega_\phi = 2.5$ and 10.0 which uses time variant trim solutions depicts the same three points observed earlier. In Figures 20

and 21, we consider the same four models for $\omega_v = 1.5$. Figure 20 shows that simplified models fail even to depict qualitatively correct trends for $\omega_\phi = 2.5$. This matter is further pursued in Figure 21 for $\omega_\phi = 5.0$ and 10.0 which shows that for $\omega_\phi = 5.0$ the rigid blade model is a poor approximation even to the CLFT model with N = 1. Only for high values of ω_ϕ ($\omega_\phi \geq 10.0$), the three simplified models depict qualitatively correct trends. Thus, the gist of the data presented in Figures 18 to 21 is that the rigid blade model with quasisteady approximation to torsion can at best predict valid trends only for soft inplane configurations. As for the stiff inplane configuration this model provides useful approximations only for high torsion frequencies ($\omega_\phi \geq 10.0$). This means that most of the multiblade lag mode stability analyses under hub-fixed and hub-free conditions warrant further validation on the basis of the MFL or the base-line configuration.

Finally we come to Figure 22 for a qualitative insight into effects of dynamic inflow on the first lag mode damping. Since it is a low-frequency mode, the damping levels are expected to be affected by dynamic inflow[4,9,11,13]. However, with the present state-of-the-art there is no viable dynamic inflow model applicable to a single bladed rotor which lacks polar symmetry[13]. The method of equivalent Lock number and drag coefficient or the '$\gamma^* - C_d^*$' method is applicable only to low-frequency regressing modes. In the present case, in the absence of the regressing modes, the application of the '$\gamma^* - C_d^*$' method should be viewed as an empirical approach. In spite of such limitations, the data presented in Figure 22 (for R = 0.0 and 1.0 in combination with $\omega_\phi = 10.0$) do indicate that with increasing advance ratio the effect of dynamic inflow decreases, an observation consistent with the physics of dynamic inflow[13]. It is also seen that the effects of dynamic inflow are not negligible, particularly in the low advance ratio range ($0 \leq \mu \leq 0.25$).

V. Concluding Remarks

The modified elastic lag-flap or the MFL model is based on the fact that in the torsion equations, torsional structural terms dominate the torsional dynamic terms (inertia and damping). Numerical results in forward flight ($0 \leq \mu \leq 0.4$) show that this model goes well beyond the rigid lag-flap model with quasisteady approximation to torsion and that it provides a viable alternative to the base-line model (CLFT model with N = 2) for soft inplane rotors. This means, as a conceptual model, it is satisfactory practically for all hingeless rotor blade configurations which usually have soft inplane rotors[16]. By comparison to the base-line model, it has fewer degrees of freedom and is so much simpler. Therefore, the additions of important effects from control flexibility, control feedback, dynamic inflow, airframe coupling etc., in multiblade analyses in forward flight become manageable.

Numerical results further demonstrate the following:

(1) For soft inplane rotors, only the CLFT model with N = 1 is comparable to the rigid lag-flap model with quasisteady approximation to torsion. These two models can at best provide only qualitative approximation to the base-line model. However, their tractability in multiblade lag mode stability analyses with airframe coupling etc., may outweigh this fact.

(2) The inclusion of dynamic inflow by the empirical use of '$\gamma^* - c_d^*$' method indicates that the inflow effects may be appreciable, particularly in the low advance ratio range ($0 \leq \mu \leq 0.25$).

(3) For stiff inplane rotor blades, except for $\omega_\phi \geq 5.0$, it is difficult to characterise the effect of torsion dynamics in a simpler manner. For such cases, a coupled lag-flap-torsional model may be necessary to account for torsion dynamics in a reliable manner. However, for $\omega_\phi \geq 5.0$, the MFL model is satisfactory. Only for high values of ω_ϕ ($\omega_\phi \geq 10.0$), the rigid blade model with quasisteady approximation to torsion is qualitatively accurate.

(4) For the base-line configuration with stiff inplane blades, which are excessively flexible torsionally (say, $\omega_\phi \leq 3.0$) the sudden degradation in stability margin in the high advance ratio range ($\mu \geq 0.25$) merits further investigation. And so is the case for matched stiffness frequency values of the base-line configuration for all values of ω_ϕ ($2.5 \leq \omega_\phi \leq 10.0$). For this matched stiffness case, in hover[2,15], the lag mode damping values though agree with those of reference 2, indicate subtle differences with those of reference 15.

References

1) Friedmann, P. Peretz, "Formulation and Solution of Rotary Wing Aeroelastic Stability and Response Problems", Vertica, Vol.7, No.2, 1983, pp.101-141.

2) Hodges, H. Deway, and R.A. Ormiston, Stability of Elastic Bending and Torsion of Uniform Cantilever Rotor Blades in Hover with Variable Structural Coupling, NASA TN D-8192, April 1976.

3) P.P. Friedmann, and S.B.R. Kottapalli, "Coupled Flap-Lag-Torsional Dynamics of Hingeless Rotor Blades in Forward Flight", Journal of the American Helicopter Society, Vol.27, No.4, October 1982, pp.28-36.

4) G.H. Gaonkar, A.K. Mitra, and D.A. Peters, "Feasibility of a Rotor Flight Dynamics Model with First Order Cyclic Inflow and Multiblade Modes", AIAA Dynamics Specialists Meeting, Atlanta, Georgia, April 9-10, 1981, AIAA Paper No. 81-0611-CP.

5) H.C. Curtiss, Jr., "Sensitivity of Hingeless Rotor Blade Flap-Lag Stability in Hover to Analytical Modelling Assumptions", AMS Report No.1236, Princeton University, Department of Aerospace and Mechanical Sciences, January 1975.

6) J. Dugundji and J.H. Wendell, "Some Analysis Methods for Rotating Systems with Periodic Coefficients", AIAA Journal, Vol.21, No.6, June 1983, pp.891-897.

7) G.H. Gaonkar, D.S. Simha Prasad and D. Sastry, "On Computing Floquet Transition Matrices of Rotorcraft", The Journal of the American Helicopter Society, Vol.26, No.3, July 1981, pp.29-36.

8) J. Nagabhushanam and G.H. Gaonkar, "Rotorcraft Air Resonance in Forward Flight with Various Dynamic Inflow Models and Aeroelastic Couplings", Ninth European Rotorcraft Forum, Stresa, Italy, September 13-15, 1983, paper No.52 (Also see VERTICA, Vol.4, No.7, 1984).

9) G.H. Gaonkar, A.K. Mitra, T.S.R. Reddy and D.A. Peters, "Sensitivity of Helicopter Aeromechanical Stability to Dynamic Inflow", Vertica, Vol.6, 1982, pp.59-75.

10) G.H. Gaonkar, K.H. Hohenemser and S.K. Yin, "Random Gust Response Statistics for Coupled Torsion Flapping Rotor Blade Vibrations", Journal of Aircraft, Vol.9, No.10, October 1972, pp.726-729.

11) D.A. Peters and G.H. Gaonkar, "Theoretical Flap-Lag Damping with Various Dynamic Inflow Models", Journal of the American Helicopter Society, Vol.25, No.3, July 1980, pp.29-36.

12) G.H. Gaonkar and D.A. Peters, "Use of Multiblade Coordinates for Helicopter Flap-Lag Stability with Dynamic Inflow", Journal of Aircraft, Vol.17, No.2, February 1980, pp.112-119.

13) G.H. Gaonkar, V.S.S.S. Sastry, T.S.R. Reddy, J. Nagabhushanam and D.A. Peters, "The Use of Actuator-Disk Dynamic Inflow for Helicopter Flap-Lag Stability", Journal of the American Helicopter Society, Vol.28, No.3, July 1983, pp.79-88.

14) G.R. Neelakantan, Feasibility of Simplifying Coupled Lag-Flap-Torsion Models for Rotor Blade Stability in Forward Flight, M.Sc. Thesis, Indian Institute of Science, Bangalore-560 012, India (to be submitted).

15) T.S.R. Reddy, "Flap-Lag Damping of an Elastic Rotor Blade with Torsion and Dynamic Inflow in Hover from Symbolically Generated Equations", AIAA/ASME/ASCE/AHS 25th SSDM Conference, May 14-16, Palm Springs, California, Paper No. AIAA-84-0989.

16) W.G. Bousman, R.A. Ormiston and M.H. Paul, "Design Considerations for Bearingless Rotor Hubs", 39th Annual Forum of the American Helicopter Society, St.Louis, Missouri, May 1983, pp.509-536.

17) S.P. King, "Theoretical and Experimental Investigations into Helicopter Air Resonance", 39th Annual Forum of the American Helicopter Society, May 9-11, 1983, Preprint No. A-83-39-21-3000.

18) J. Nagabhushanam, G.H. Gaonkar and T.S.R. Reddy, "Automatic Generation of Equations for Rotor-Body Systems with Dynamic Inflow for a priori Ordering Schemes", Paper No.37, 7th European Rotorcraft Forum, Garmisch-Partenkirchen, West Germany, 1981.

Symbols

a	:	Airfoil lift curve slope
c	:	blade chord
c_{d_0}	:	airfoil profile drag coefficient
$c^*_{d_0}$	:	equivalent drag coefficient
C_W	:	thrust coefficient

E	:	Young's Modulus
G	:	Shear modulus
J	:	torsional stiffness constant
k_A	;	polar radius of gyration of blade cross-section
k_m	:	mass radius of gyration of blade cross-section
k_{m_1}, k_{m_2}	:	principal mass radii of gyration
m	:	mass of blade per unit length
N	:	number of non-rotating modes for flap bending, lag bending and torsional degrees of freedom (equal number of modes for flap, lag and torsion).
$\bar{R}$	:	blade radius
R	:	flap-lag coupling parameter
u, v, w	:	displacements of the elastic axis in the x, y, z directions respectively
V_j	:	generalized co-ordinate for lag degree of freedom
W_j	:	generalized co-ordinate for flap degree of freedom
V_{0_j}	:	time dependent equilibrium quantity of lead-lag mode
W_{0_j}	:	time dependent equilibrium quantity for flap mode
x, y, z	:	undeformed co-ordinate system
x', y', z'	:	deformed co-ordinate system fixed to blade
Ω	:	angular velocity
θ	:	pitch angle
γ	:	Lock number
γ^*	:	equivalent Lock number
λ	:	inflow ratio
ρ	:	density
θ_0	:	collective pitch angle
θ_s, θ_c	:	cyclic pitch components
μ	:	advance ratio
σ	:	blade solidity

ψ : azimuth angle

θ_β, θ_ζ : equivalent kinematic pitch-flap and pitch-lag coupling parameters

ψ_j : non-rotating flap and lead-lag bending mode shapes

θ_j : non-rotating torsional mode shape

Φ_{0j} : time dependent equilibrium quantity of torsion mode

ϕ : elastic torsion deflection

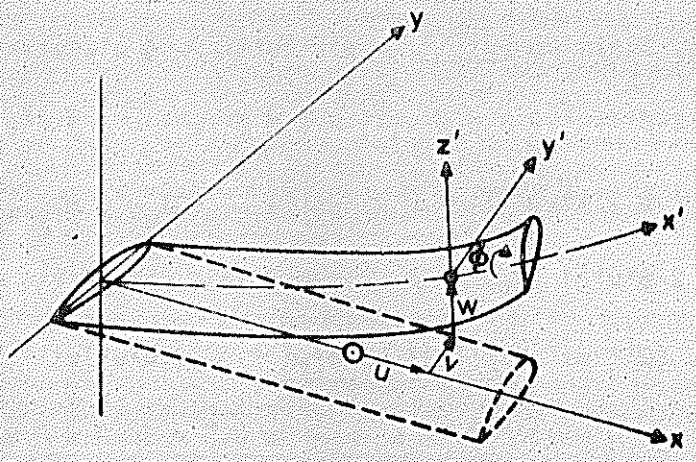

FIG. 1. BLADE GEOMETRY WITH DISPLACEMENTS.

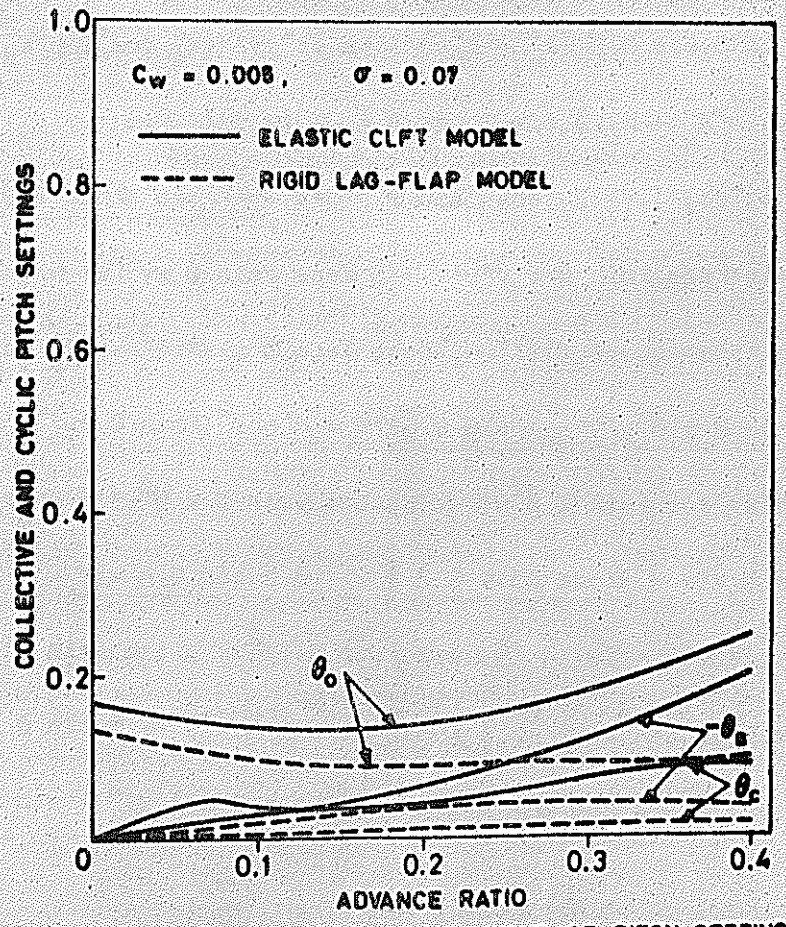

FIG. 2. PROPULSIVE TRIM SOLUTIONS OF PITCH SETTING IN HOVER & FORWARD FLIGHT.

Appendix A

As an illustrative example, we present in the sequel the lag equation in which sin θ and cos θ are not assigned a specific order of magnitude, although θ is $O(\epsilon)$. The manually generated equations agree with the symbolically generated equations from the method of reference 18.

Lag equations:

$$(EI_{z'}\cos^2\theta + EI_{y'}\sin^2\theta)\,(v'''' + 3\,v''w'''w''' + v'w'w'''' + v''w'w''' + v''w''w'' + 4\,v'v''v''' + v'v'v'''' + v''v''v'')$$

$$+(EI_{z'} - EI_{y'})\,\tfrac{1}{2}\sin 2\theta\,(w'''' + w''w'''w''' + \tfrac{1}{2}\,w'w'w'''' - 4\,\phi'v''' - 2\,\phi v'''' - 2\,\phi''v''' - 8\,\phi\,\phi'w''' - 4\,\phi\,\phi''w'' - 4\,\phi'\phi'w'' - 2\,\phi^2w'''' + \tfrac{1}{2}\,v''v'w'''' + v''v''w''') + (EI_{z'} - EI_{y'})\cos 2\theta\,(\phi w'''' + 2\,\phi'w''' + \phi''w'' - 4\,\phi\,\phi'v''' - 2\,\phi\phi'v''' - 2\,\phi'\,\phi'v'' - \phi^2v'') + GJ\,(\phi'''w' + \phi''w'' + \phi'w''' + 4\,w'w''v''' + 2\,w'w'''v'' + 2\,w''w''v'' + w'w'v'''') + m\,\ddot{v} - m\,\Omega^2 v + 2\,m\,\Omega\,\dot{u}$$

$$+\{-m\,\ddot{v}'\,(k_{m_2}^2\cos^2\theta + k_{m_1}^2\sin^2\theta) - m\,\ddot{w}'\,(k_{m_2}^2 - k_{m_1}^2)\sin\theta\cos\theta + 2\,m\,\Omega\sin\theta\cos\theta\,\dot{\phi}\,(k_{m_2}^2 - k_{m_1}^2) + m\,\Omega^2 v'\,(k_{m_2}^2\cos^2\theta + k_{m_1}^2\sin^2\theta) + m\,\Omega^2 w'\,(k_{m_2}^2 - k_{m_1}^2)\sin\theta\cos\theta\}' - (v'T)' =$$

$$(a\rho\bar{R}^3\Omega^2\tfrac{1}{2}c)\,[(-2\mu\cos\psi\sin\theta\,v'w'v - \mu^2\cos^2\psi\cos\theta\,\phi v'w' + \tfrac{1}{2}\mu^2\sin\psi\cos\psi\sin\theta\,v'v'w' + \tfrac{1}{2}\mu\cos\psi\sin\theta\,xv'^2w' - \mu^2\sin\psi\cos\psi\cos\theta\,v'w'^2 - \mu\cos\psi\cos\theta\,x\,v'w'^2 + 2\mu\cos\psi\cos\theta\,w'^2v - \mu\sin\psi\cos\theta\,\phi\,w'v - \cos\theta\,x\,\phi w'v - \mu^2\cos^2\psi\sin\theta\,\phi w'^2 + \tfrac{1}{2}\mu^2\sin\psi\cos\psi\sin\theta\,\phi^2w' + \tfrac{1}{2}\mu\cos\psi\sin\theta\,x\,\phi^2w' - \mu\cos\psi\sin\theta\,w'w - \lambda\sin\theta\,v'v - \mu\cos\psi\cos\theta\,\lambda\,\phi\,v' + 2\cos\theta\,\lambda\,w'v - 2\mu\cos\psi\sin\theta\,\lambda\,\phi w' + \tfrac{1}{2}\mu\sin\psi\sin\theta\lambda\phi^2 + \mu\sin\psi\sin\theta\,\lambda\,v'^2 - \mu\sin\psi\cos\theta\,\lambda\,v'w' + \tfrac{1}{2}\,\mu\sin\psi\sin\theta\,\lambda\,w'^2 + \tfrac{1}{2}\sin\theta\,\lambda\,x\,\phi^2 - \sin\theta\,\lambda\,x\,v'^2 - \cos\theta\,\lambda\,x\,v'w' + \tfrac{1}{2}\sin\theta\,x\,\lambda\,w'^2 - \sin\theta\,\lambda\,u -$$

$$-\sin\theta\,\lambda^2\,\phi - \mu^2\cos^2\psi\sin\theta\,v'w' + \mu\sin\psi\sin\theta\,v'^2 -$$

$$\mu\sin\psi\sin\theta\,w'v - \sin\theta\,x\,w'v + \mu^2\cos^2\psi\cos\theta\,w'^2 -$$

$$\mu^2\sin\psi\cos\psi\cos\theta\,\phi\,w' - \mu\cos\psi\cos\theta\,x\,\phi\,w' -$$

$$\mu\cos\psi\sin\theta\,\lambda\,w' + 2\,\mu\cos\psi\cos\theta\,\lambda\,w' - \mu\sin\psi\cos\theta\,\lambda\,\phi -$$

$$\cos\theta\,\lambda\,x\,\phi + \cos\theta\,\lambda^2 - \mu^2\sin\psi\cos\psi\sin\theta\,w' -$$

$$\mu\cos\psi\sin\theta\,x\,w' - \mu\sin\psi\sin\theta\,\lambda - \sin\theta\,x\,\lambda\,)$$

$$+(c_{d_0}/a)\,(-\mu^2\sin\psi\cos\psi\sin\theta\,w' - \mu\cos\psi\sin\theta\,x\,w'$$

$$+\mu^2\sin^2\psi\sin\theta\,\phi + 2\mu\sin\psi\sin\theta\,x\,\phi + \sin\theta\,x^2\,\phi -$$

$$2\mu^2\sin\psi\cos\psi\cos\theta\,v' - 2\mu\cos\psi\cos\theta\,x\,v' -$$

$$\mu\sin\psi\sin\theta\,\lambda - \sin\theta\,x\,\lambda - \mu^2\sin^2\psi\cos\theta - 2\mu\sin\psi\,x\cos\theta -$$

$$x^2\cos\theta\,) + (-\sin\theta\,v'v\dot{w} - \mu\cos\psi\cos\theta\,\phi\,v'\,\dot{w}$$

$$+\mu\sin\psi\sin\theta\,w'\,\dot{u} + \sin\theta\,x\,w'\,\dot{u} - \sin\theta\,w'\,v\,\dot{v} -$$

$$\mu\cos\psi\cos\theta\,\phi\,w'\,\dot{v} - 2\mu\cos\psi\sin\theta\,\phi\,w'\,\dot{w} - \cos\theta\,\phi\,\dot{v}\,\dot{w}$$

$$+\tfrac{1}{2}\mu\sin\psi\sin\theta\,\phi^2\,\dot{w} - \mu\sin\psi\cos\theta\,v'\,w'\,\dot{w}$$

$$+\tfrac{1}{2}\mu\sin\psi\sin\theta\,w'^2\,\dot{w} + \tfrac{1}{2}\sin\theta\,x\,\phi^2\,\dot{w} - \sin\theta\,x\,v'^2\,\dot{w} -$$

$$\cos\theta\,x\,v'\,w'\,\dot{w} + \tfrac{1}{2}\sin\theta\,x\,w'^2\,\dot{w} - \sin\theta\,u\,\dot{w} - \sin\theta\,\phi\,\dot{w}^2$$

$$+2\cos\theta\,w'\,v\,\dot{w} + \mu\sin\psi\sin\theta\,v'^2\,\dot{w} + \sin\theta\,x\,w'\,\dot{u} -$$

$$\cos\theta\,\lambda\,\phi\,\dot{v} - 2\sin\theta\,\lambda\,\phi\,\dot{v} - 2\sin\theta\,\lambda\,\phi\,\dot{w} - \mu\cos\psi\sin\theta\,v'\,\dot{w} -$$

$$\mu\cos\psi\sin\theta\,w'\,\dot{v} - \sin\theta\,\dot{v}\,\dot{w} - \mu\sin\psi\cos\theta\,\phi\,\dot{w} -$$

$$\cos\theta\,x\,\phi\,\dot{w} + 2\,\mu\cos\psi\cos\theta\,w'\,\dot{v} + \sin\theta\,\dot{v}^2$$

$$+\cos\theta\,\dot{w}^2 - \sin\theta\,\lambda\,\dot{v} + 2\cos\theta\,\lambda\,\dot{w} - \mu\sin\psi\sin\theta\,\dot{w} -$$

$$\sin\theta\,x\,\dot{w}\,) + (c_{d_0}/a)\,(-2\,x\cos\theta\,\dot{v} - 2\,\mu\sin\psi\sin\theta\,\dot{v} -$$

$$-\sin\theta \times \ddot{\bar{w}} - 2\mu\sin\psi\cos\theta\,\dot{\bar{v}} - 2\cos\theta \times \dot{\bar{v}} - \mu\sin\psi\sin\theta\,\dot{\bar{w}}\,)$$

$$+\left(\tfrac{3}{4}c\right)\left(-\lambda\dot{\phi} - \ddot{\bar{w}}\,\dot{\phi} + x\,\phi\,\dot{\phi} + \mu\sin\psi\,\phi\,\dot{\phi} - \mu\cos\psi\,w'\,\dot{\phi}\,\right)$$

$$+\left(\tfrac{1}{2}c\right)\left(-\lambda w' - w'\,\ddot{\bar{w}} + x\,\phi\,w' + \mu\sin\psi\,\phi\,w' - \mu\cos\psi\,w'\,w'\right)$$

$$+\left(\tfrac{1}{4}c\right)\left(-\sin\theta\cos\theta\,\ddot{\bar{w}}' + x\sin\theta\cos\theta\,\dot{\phi} + \mu\sin\psi\sin\theta\cos\theta\,\dot{\phi} - \mu\cos\psi\sin\theta\cos\theta\,\dot{\bar{w}}'\right)\Big]$$

.....A1

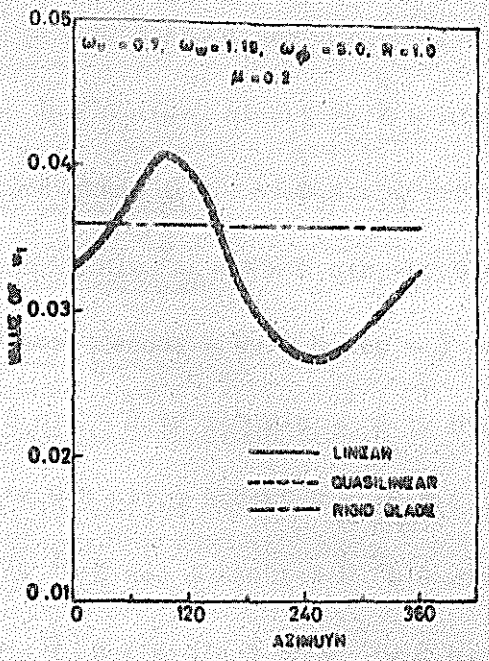

FIG. 3. RESPONSE OF THE FIRST FLAP MODE.

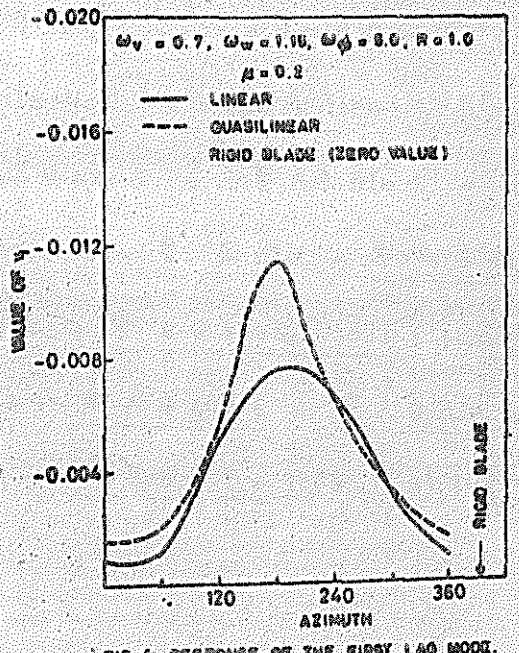

FIG. 4. RESPONSE OF THE FIRST LAG MODE.

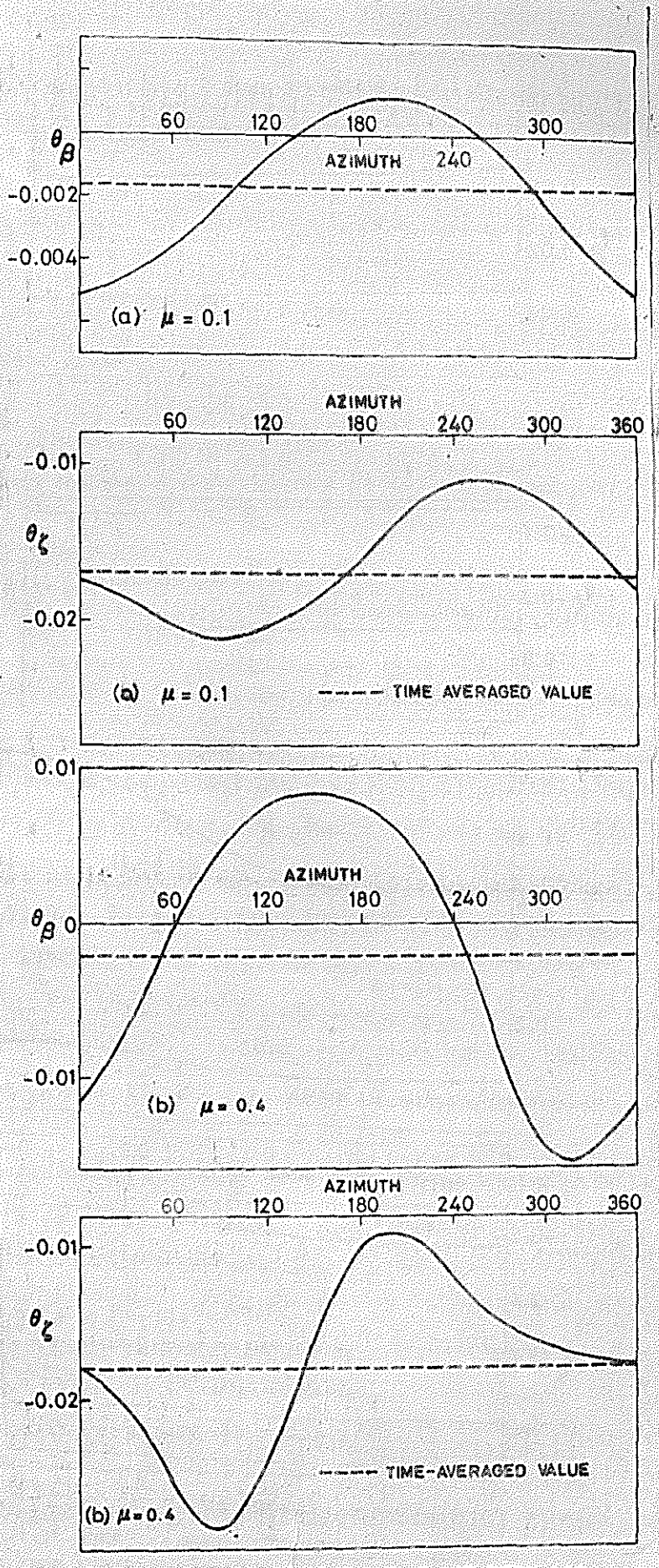

FIG. 8. VARIATION OF PITCH-FLAP AND PITCH-LAG COUPLINGS Vs. AZIMUTH (ω_v = 0.7, ω_w = 1.15, R = 1, ω_ϕ = 10).

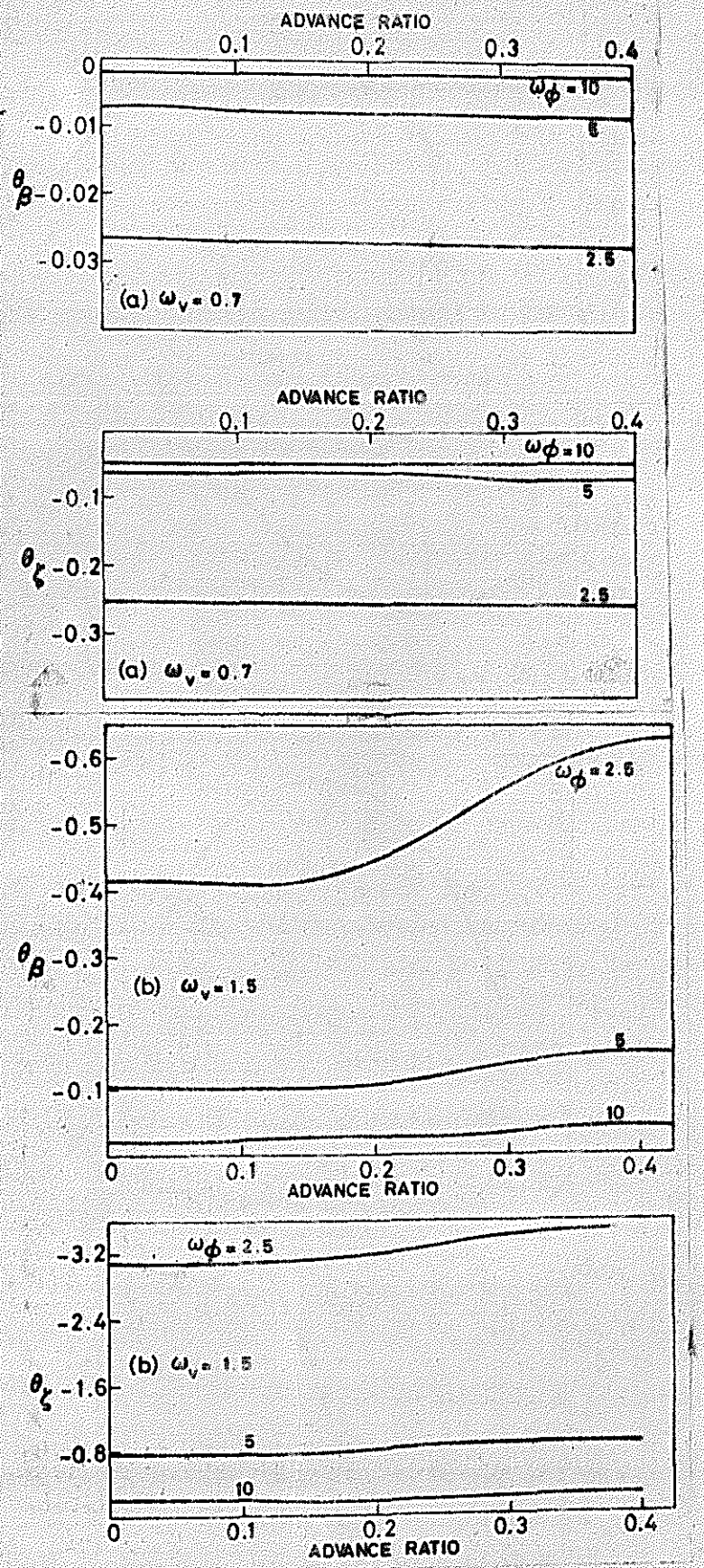

FIG. 6. TIME AVERAGED EQUIVALENT PITCH-FLAP AND PITCH-LAG COUPLINGS FOR A SOFT & STIFF INPLANE BLADES Vs. ADVANCE RATIO (R=1).

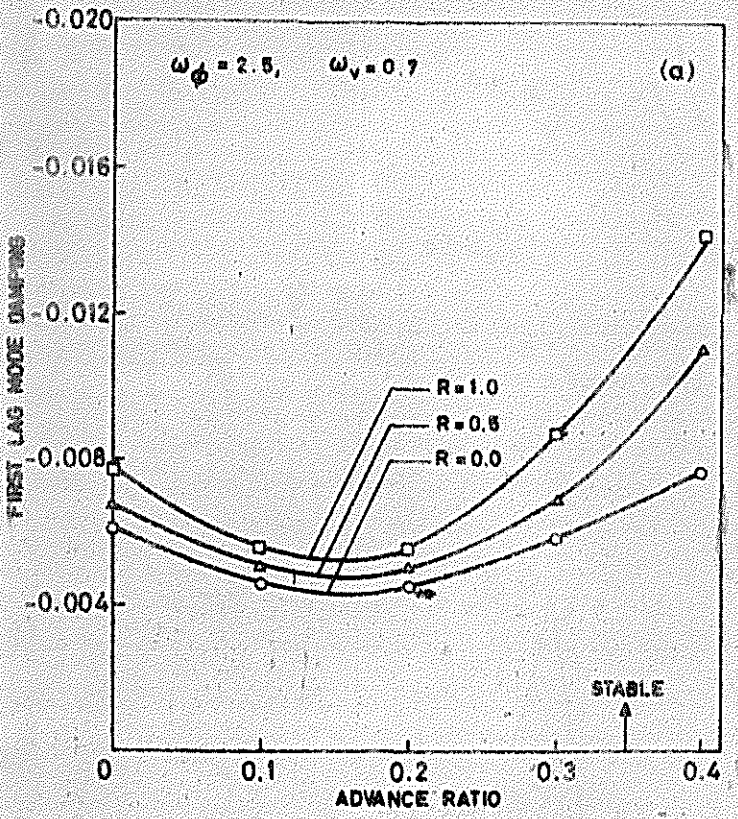

FIG. 7. FIRST LAG MODE DAMPING FOR THE BASE-LINE CONFIGURATION.

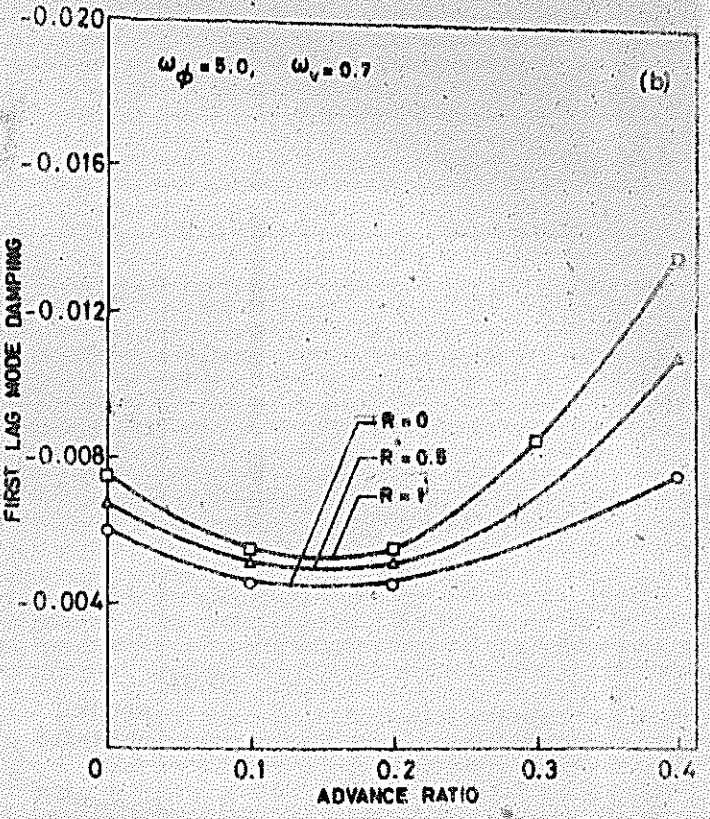

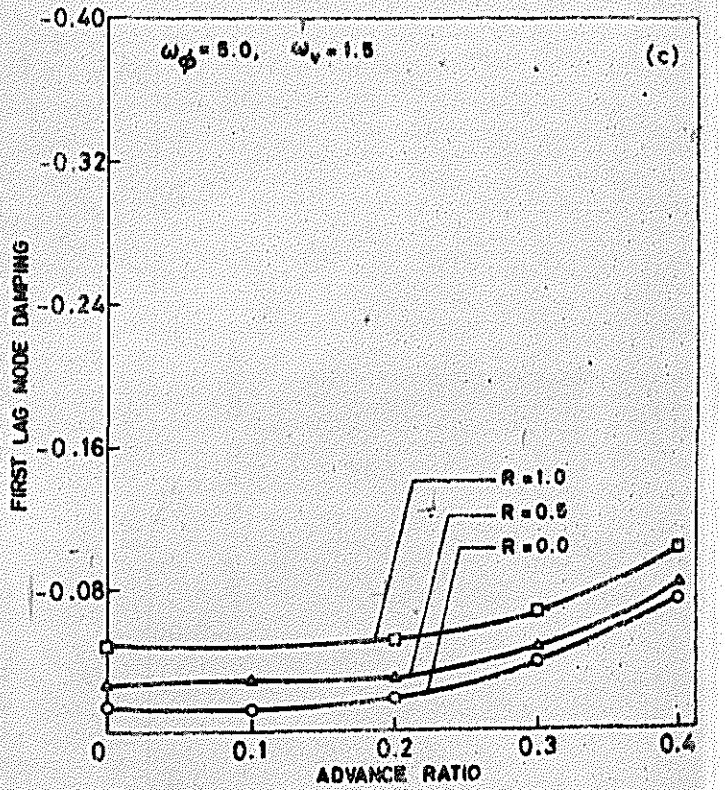

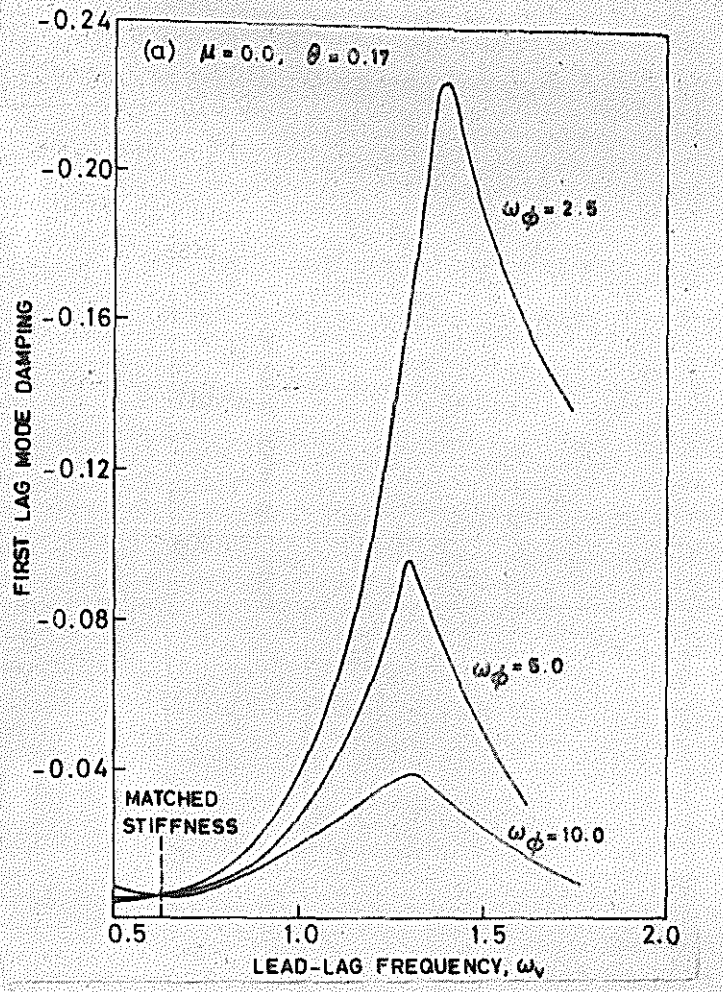

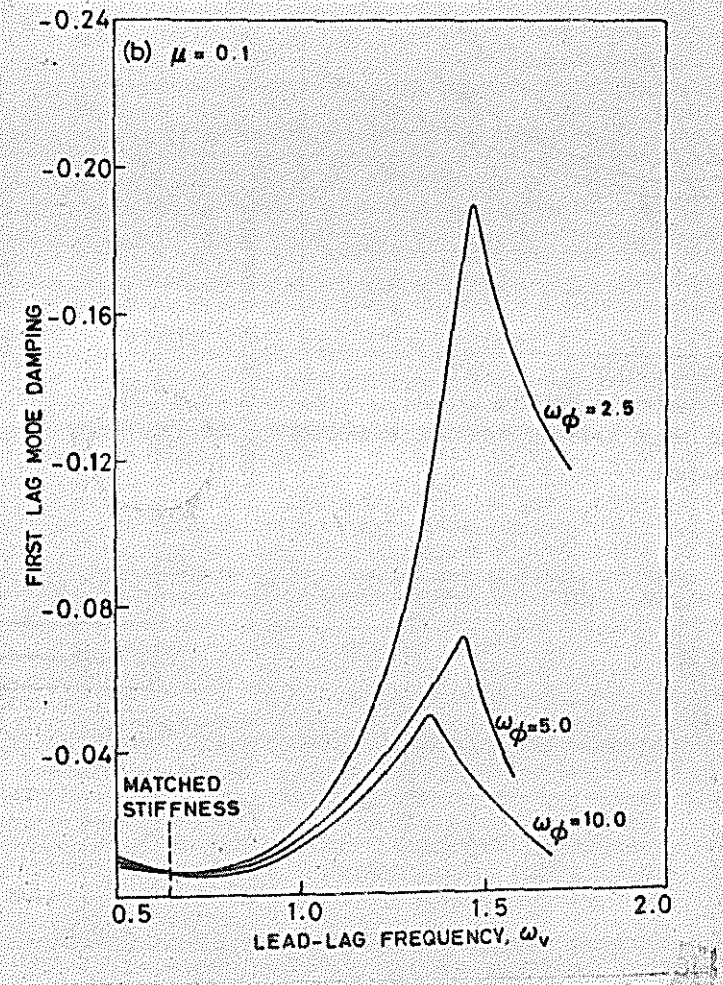

FIG. 8. THE EFFECT OF TORSION FREQUENCY ON LEAD LAG DAMPING Vs. LEAD LAG FREQUENCY AT $\mu = 0.0$ & $\mu = 0.1$ ($R = 1.0$).

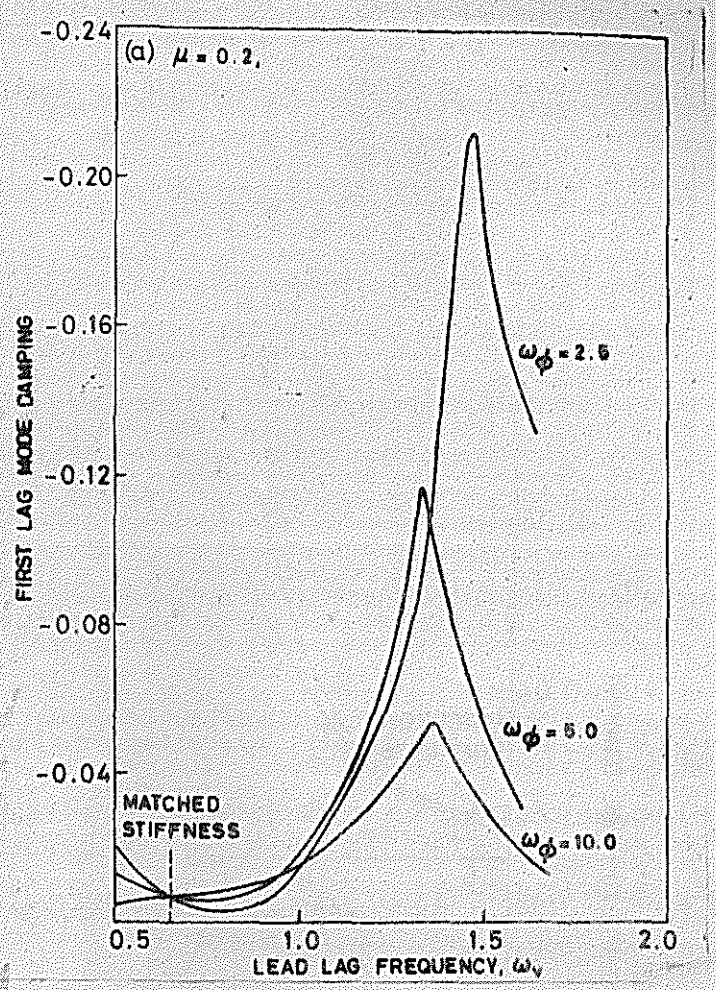

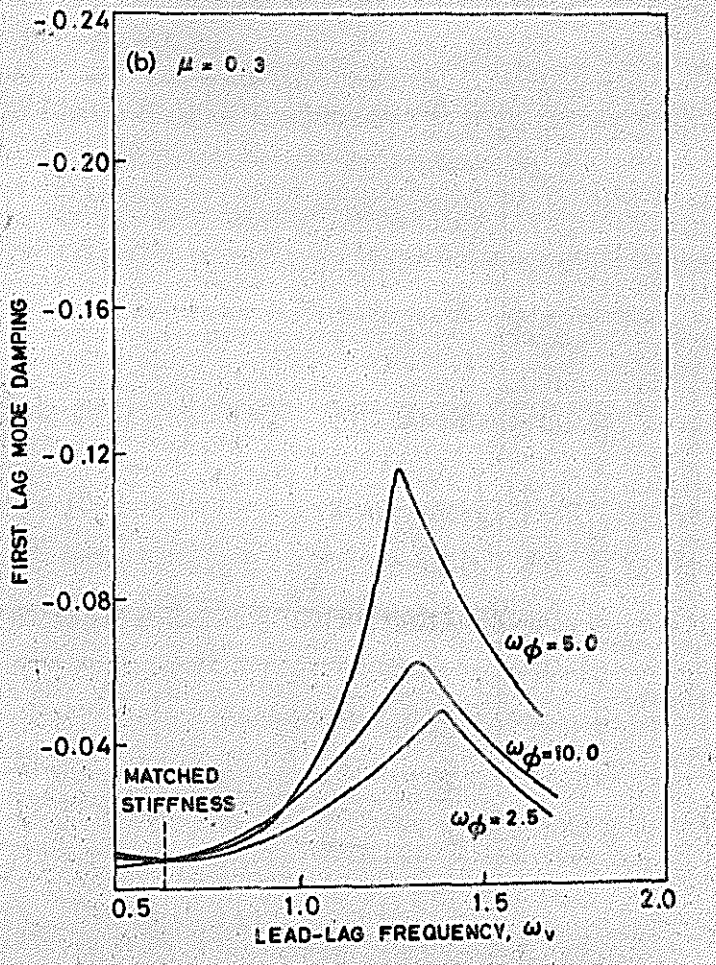

FIG. 9. THE EFFECT OF TORSION FREQUENCY ON LEAD LAG DAMPING Vs. LEAD-LAG FREQUENCY AT $\mu = 0.2$ & $\mu = 0.3$ ($R = 1.0$)

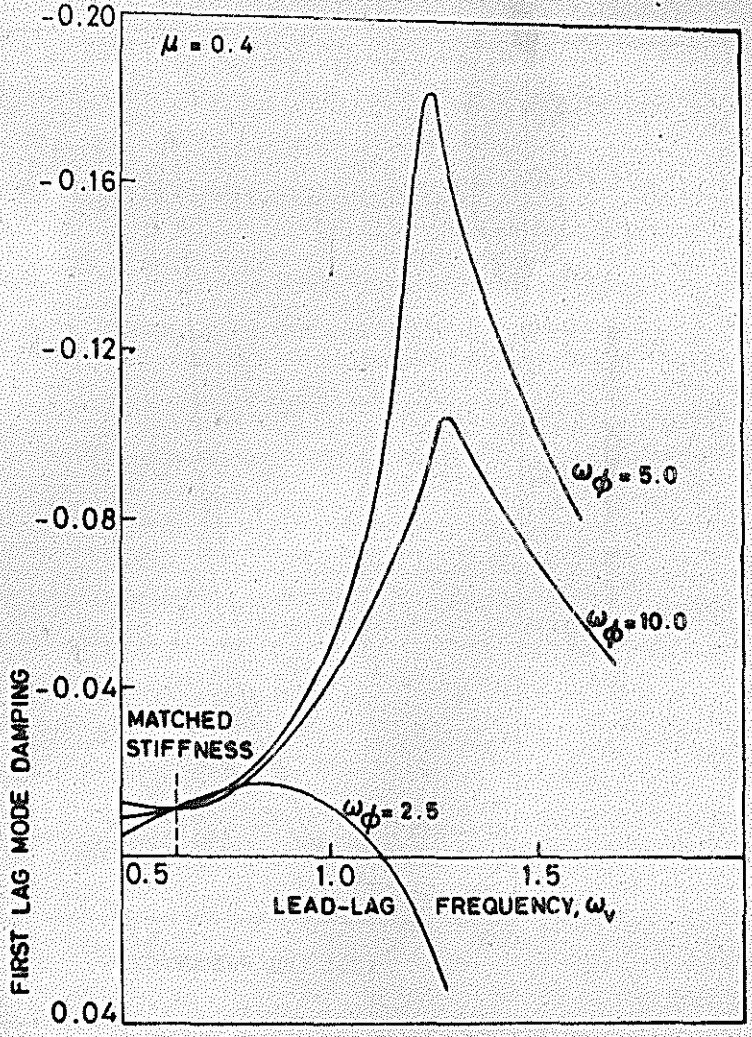

FIG. 10. THE EFFECT OF TORSION FREQUENCY ON LEAD-LAG DAMPING Vs. LEAD-LAG FREQUENCY AT $\mu = 0.4$ ($R = 1.0$)

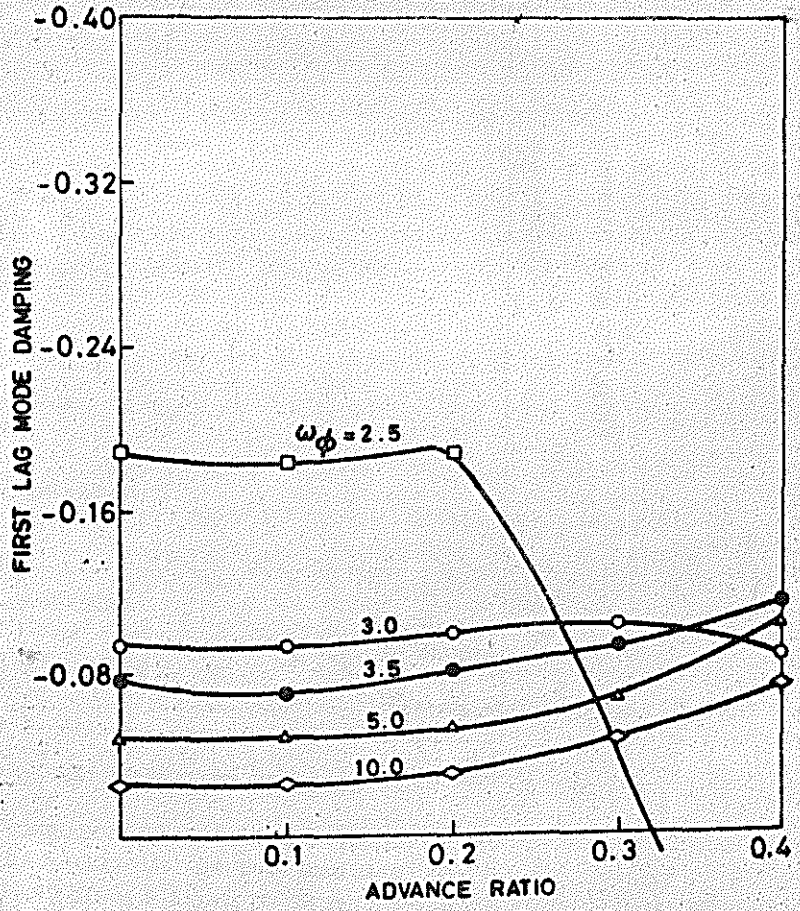

FIG. 11. LAG MODE DAMPING OF THE BASE-LINE CONFIGURATION FOR A STIFF INPLANE ROTOR.

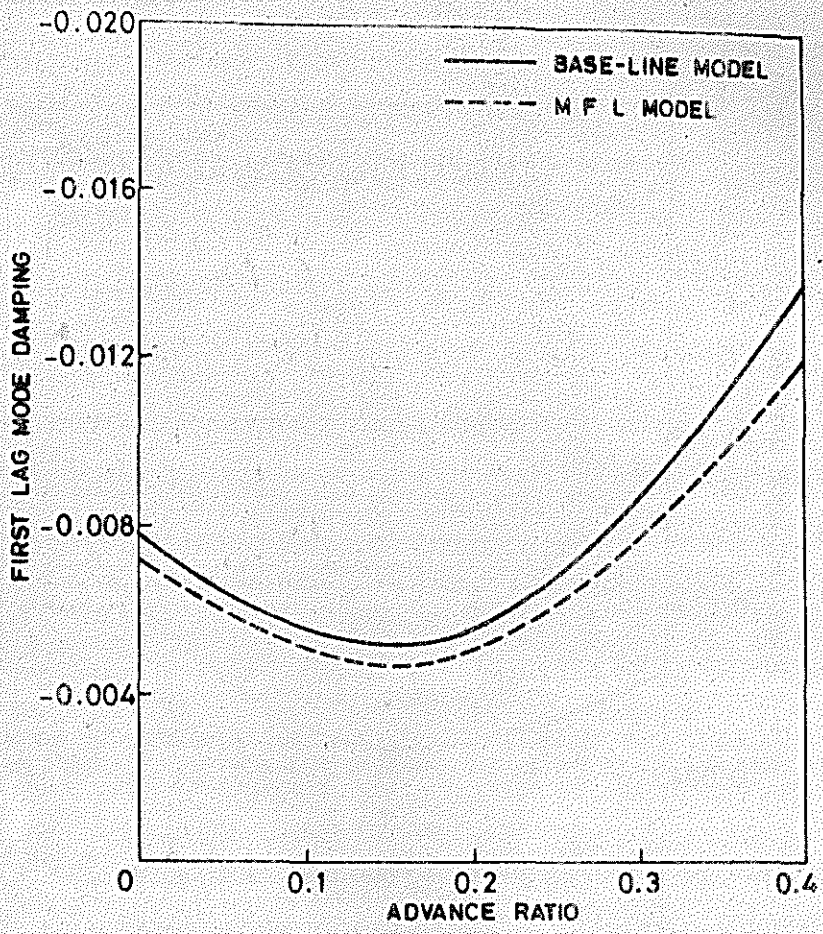

FIG. 12. COMPARISON BETWEEN BASE-LINE AND M F L MODELS FOR A SOFT INPLANE ROTOR, $\omega_\phi = 2.5$.

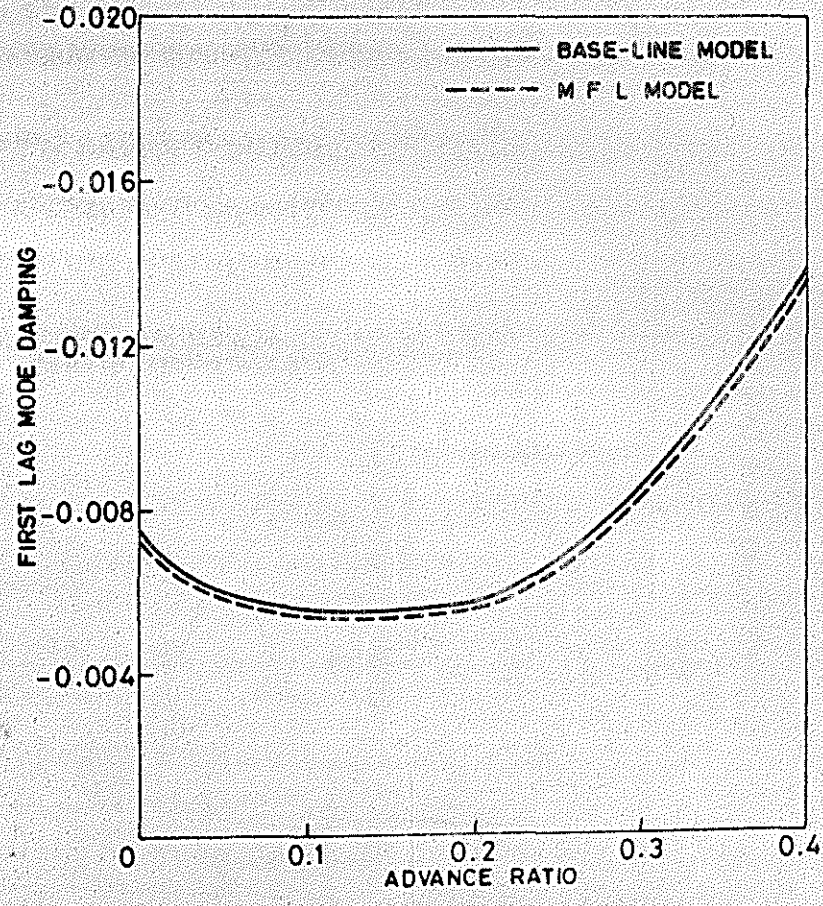

FIG. 13. COMPARISON BETWEEN BASE-LINE AND M F L MODELS FOR A SOFT INPLANE ROTOR FOR $\omega_\phi = 5.0$.

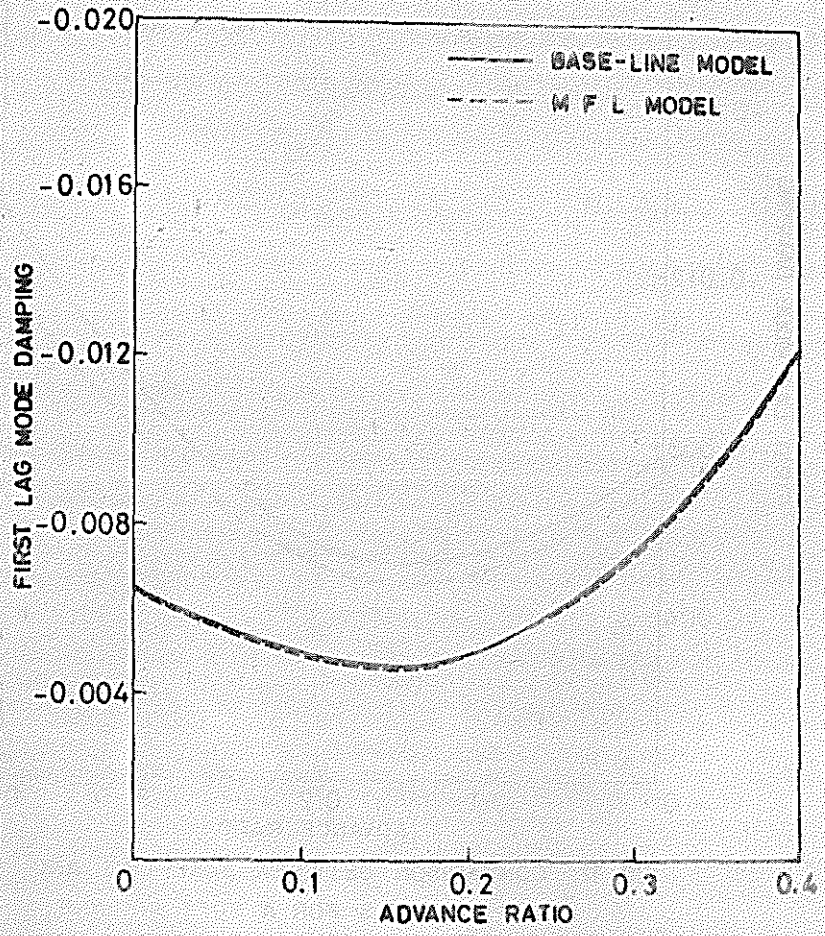

FIG. 14. COMPARISON BETWEEN BASE-LINE AND M F L MODELS FOR A SOFT INPLANE ROTOR FOR $\omega_\phi = 10$.

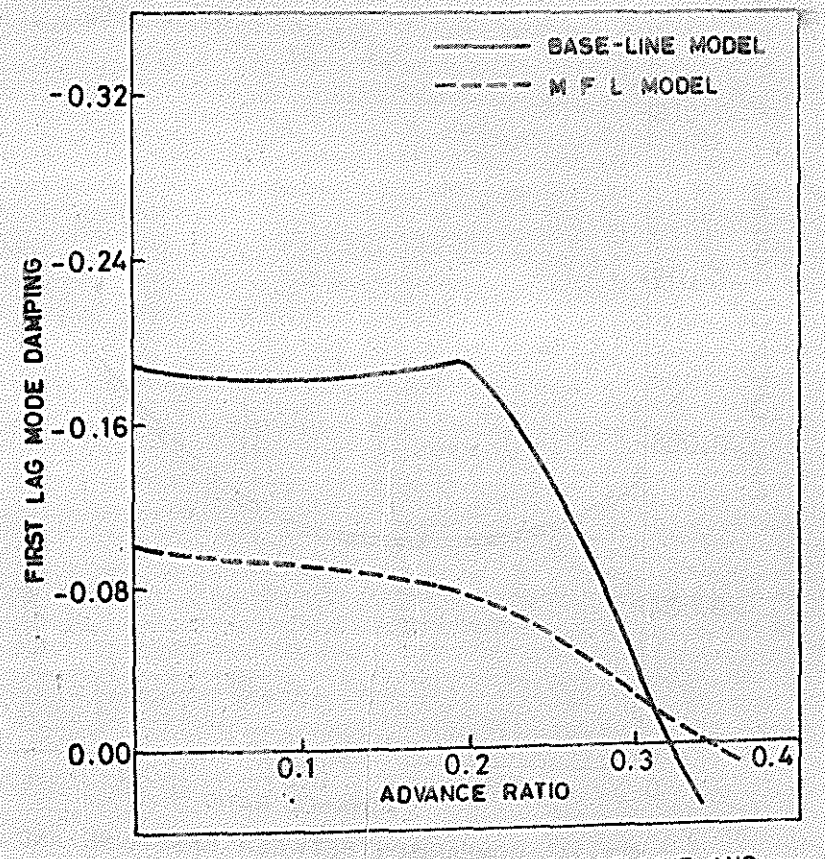

FIG. 15. COMPARISON BETWEEN BASE-LINE AND M F L MODELS FOR A STIFF INPLANE ROTOR FOR $\omega_\phi = 2.5$

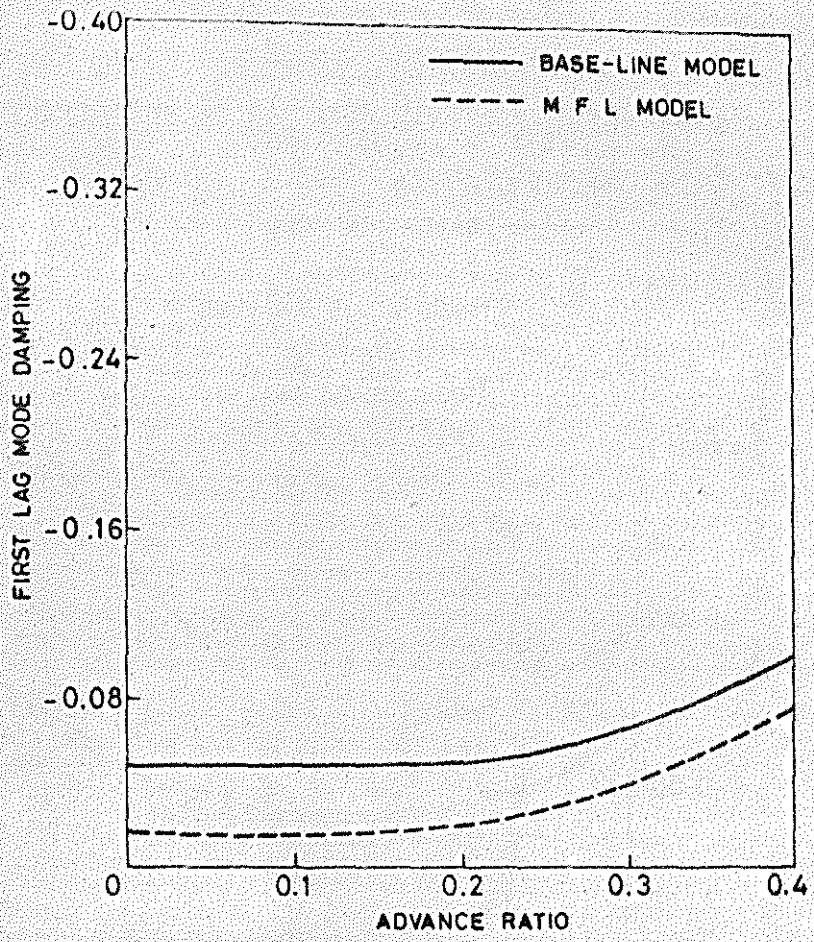

FIG. 16. COMPARISON BETWEEN BASE-LINE AND M F L MODELS FOR A STIFF INPLANE ROTOR FOR $\omega_\phi = 5$.

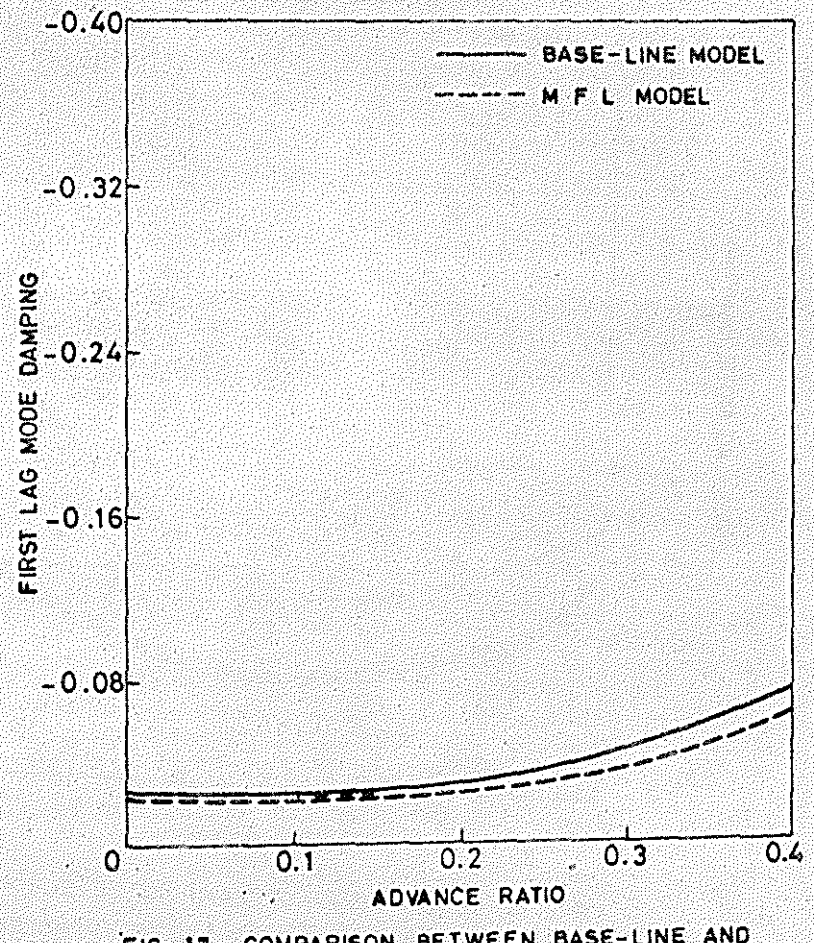

FIG. 17. COMPARISON BETWEEN BASE-LINE AND M F L MODELS FOR A STIFF INPLANE ROTOR FOR $\omega_\phi = 10.0$.

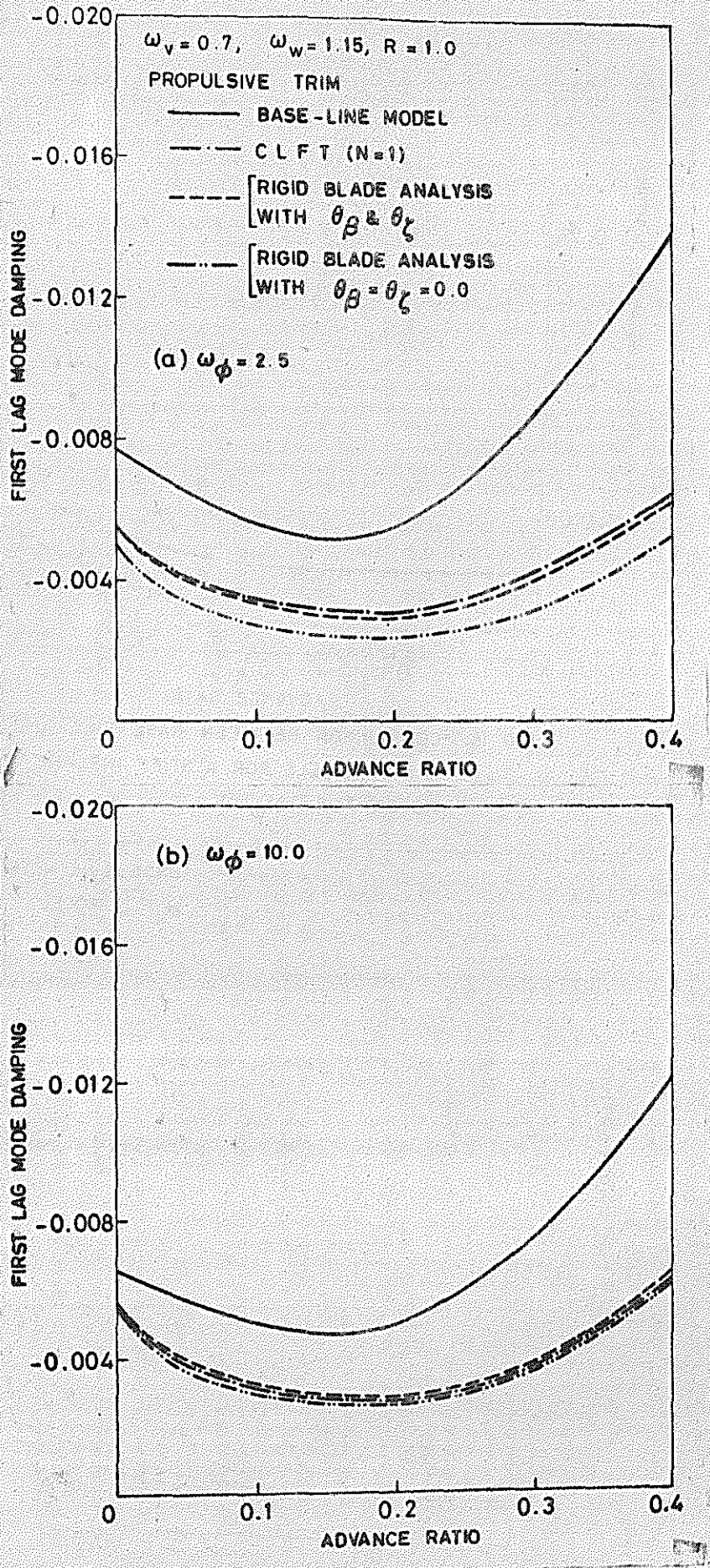

FIG. 18. COMPARISON OF DAMPING LEVELS FROM C L F T AND RIGID LAG-FLAP MODELS FOR TIME INVARIANT TRIM.

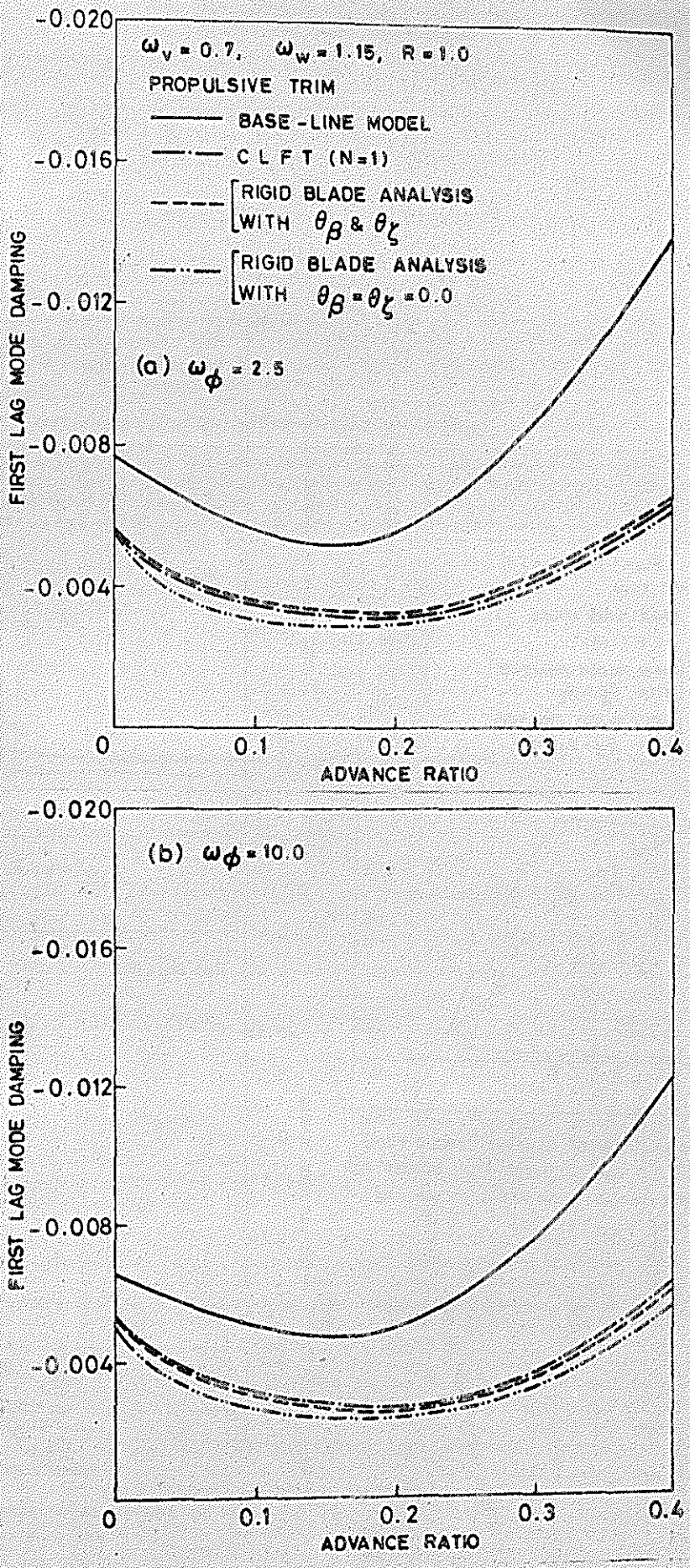

FIG. 19. COMPARISON OF DAMPING LEVELS FROM C L F T AND RIGID LAG-FLAP MODELS FOR TIME VARIANT TRIM FOR SOFT INPLANE ROTOR.

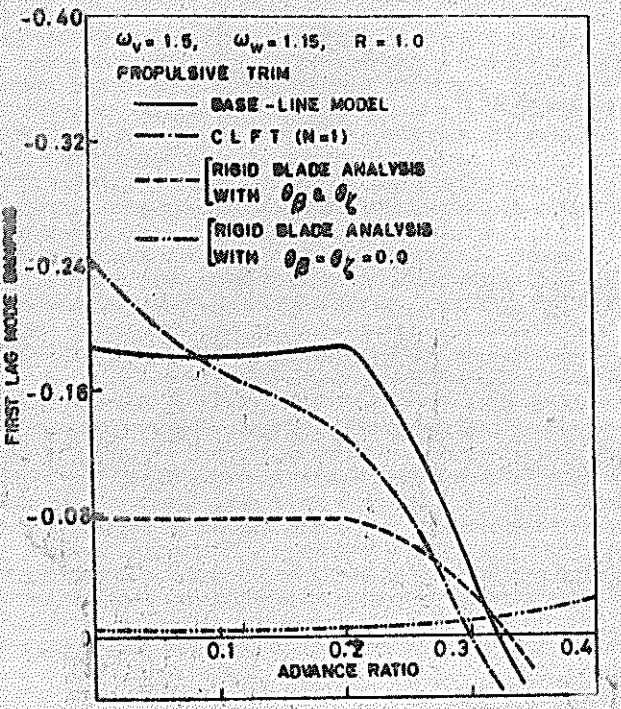

FIG. 20. COMPARISON OF DAMPING LEVELS FROM C L F T AND RIGID LAG-FLAP MODELS FOR TIME VARIANT TRIM FOR STIFF INPLANE ROTOR ($\omega_\phi = 2.5$).

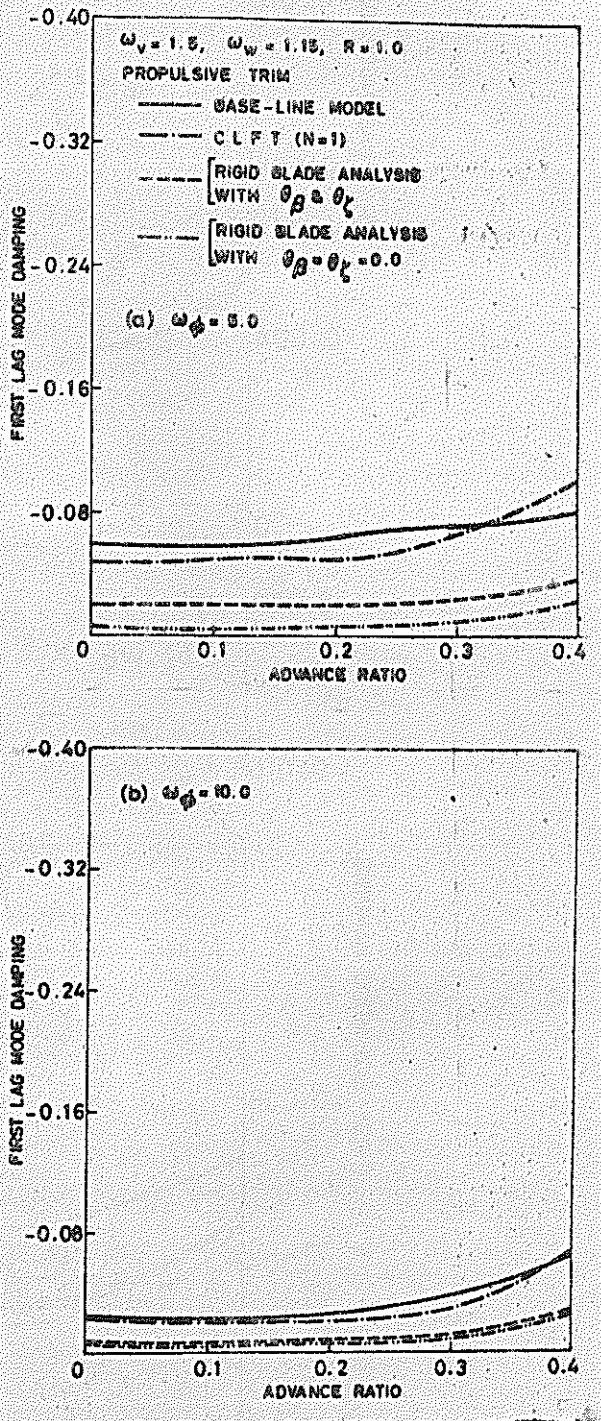

FIG. 21. COMPARISON OF DAMPING LEVELS FROM C L F T AND RIGID LAG-FLAP MODELS FOR TIME VARIANT TRIM FOR STIFF INPLANE ROTOR ($\omega_\phi = 5.0$ & 10.0)

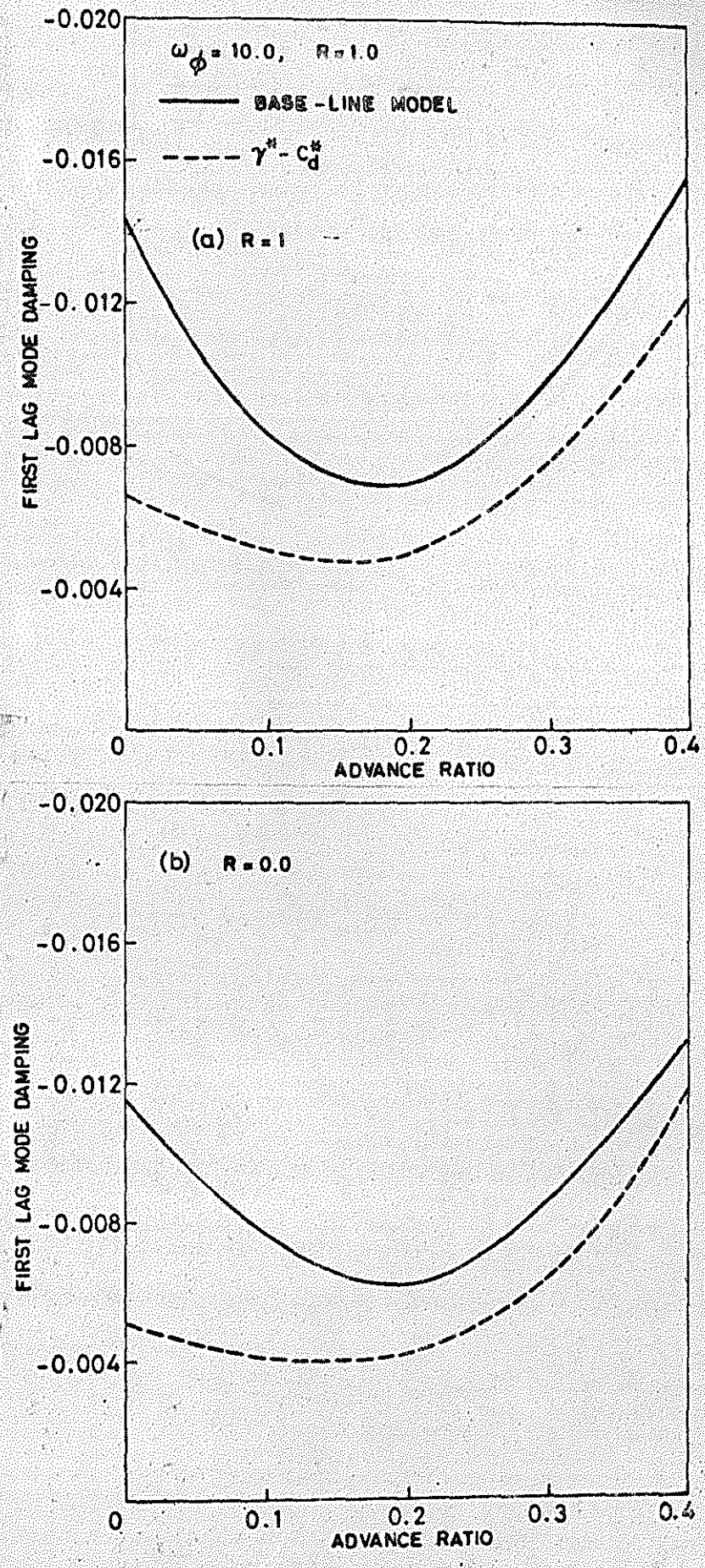

FIG. 22. EFFECT OF DYNAMIC INFLOW ON LAG MODE DAMPING.